IOP PUBLISHING JOURNAL OF PHYSICS A: MATHEMATICAL AND THEORETICAL

J. Phys. A: Math. Theor. **42** (2009) 275203 (27pp) doi:10.1088/1751-8113/42/27/275203

Short-distance expansion for the electromagnetic half-space Green's tensor: general results and an application to radiative lifetime computations

George Y Panasyuk[1], **John C Schotland**[2] **and Vadim A Markel**[3]

[1] Department of Bioengineering, University of Pennsylvania, Philadelphia, PA 19104, USA
[2] Department of Bioengineering and Graduate Group in Applied Mathematics and Computational Science, University of Pennsylvania, Philadelphia, PA 19104, USA
[3] Departments of Radiology and Bioengineering, University of Pennsylvania, Philadelphia, PA 19104, USA

E-mail: georgey@seas.upenn.edu, schotland@seas.upenn.edu and vmarkel@mail.med.upenn.edu

Received 4 August 2008, in final form 21 April 2009
Published 15 June 2009
Online at stacks.iop.org/JPhysA/42/275203

Abstract

We obtain a short-distance expansion for the half-space, frequency domain electromagnetic Green's tensor. The small parameter of the theory is $\omega\epsilon_1\mathcal{L}/c$, where ω is the frequency, ϵ_1 is the permittivity of the upper half-space, in which both the source and the point of observation are located, and which is assumed to be transparent, c is the speed of light in vacuum and $\mathcal{L}$ is a characteristic length, defined as the distance from the point of observation to the reflected (with respect to the planar interface) position of the source. In the case when the lower half-space (the substrate) is characterized by a complex permittivity ϵ_2, we compute the expansion to third order. For the case when the substrate is a transparent dielectric, we compute the imaginary part of the Green's tensor to seventh order. The analytical calculations are verified numerically. The practical utility of the obtained expansion is demonstrated by computing the radiative lifetime of two electromagnetically interacting molecules in the vicinity of a transparent dielectric substrate. The computation is performed in the strong interaction regime when the quasi-particle pole approximation is inapplicable. In this regime, the integral representation for the half-space Green's tensor is difficult to use while its electrostatic limiting expression is grossly inadequate. However, the analytical expansion derived in this paper can be used directly and efficiently. The results of this study are also relevant to nano-optics and near-field imaging, especially when tomographic image reconstruction is involved.

PACS numbers: 02.30.Gp, 03.50.De

(Some figures in this article are in colour only in the electronic version)

1. Introduction

The Green's tensor for the Maxwell equations plays a fundamental role in electromagnetic theory and optical physics. In free space, the Green's tensor is of a well-known simple form. However, when surfaces of discontinuity are present, the mathematical expression for the Green's tensor becomes rather complicated. This is true even in the simplest case of the half-space geometry. The half-space Green's tensor was derived a century ago by Sommerfeld [1] in the form of a set of oscillatory integrals (for a contemporary exposition, see [2]). Historically, the main application for Sommerfeld's work was in the theory of radiowave propagation where large-distance asymptotes are of primary interest [3]. By large distance we mean here distances large compared to the wavelength.

Recent developments in nano-optics [4] have necessitated the study of the half-space Green's tensor in the opposite limit, when the characteristic distances are small compared to the wavelength. These developments include near-field optical imaging [5–8], especially, the tomographic modalities which are based on solving the inverse scattering problem [9–15], study of surface plasmon polaritons in nanoparticle chain waveguides [16–21], or of excitons in molecular chains [22], development of sensing technologies based on control of spontaneous emission of molecules in the vicinity of nanostructures and interfaces [23–25] and radiative heat transfer on the nanoscale [26]. In each of the aforementioned examples, the physical system of interest is often deposited on a planar substrate. The substrate is typically a transparent dielectric, but can also be a metal. In either case, the Green's tensor for the half-space geometry is of central importance.

In the limit of zero frequency, the problem of computing the Green's function can be solved exactly by the method of images. The electrostatic limiting expression for the Green's tensor is well known and often used even beyond the strict statics, as long as the characteristic distances of the problem are perceived to be sufficiently small. This approach is, however, often inadequate (e.g., see [27]). One of the deficiencies of the electrostatic result is that it does not take into account radiative effects. As is well known, electromagnetic radiation is a relativistic effect which appears to third order in the dimensionless parameter $\omega\mathcal{L}/c \sim v/c$, where $\mathcal{L}$ is the characteristic distance, v is the characteristic velocity of oscillating charges and c is the speed of light in vacuum. Thus, to account for radiative effects, any expansion of the Green's tensor must be computed with at least the accuracy $\mathcal{L}^{-3}O((\omega\mathcal{L}/c)^3) = O((\omega/c)^3)$, while the electrostatic result is of the order of $\mathcal{L}^{-3}O((\omega\mathcal{L}/c)^0) = O(\mathcal{L}^{-3})$. Therefore, the electrostatic result may give the real part of the Green's tensor with sufficient accuracy but be grossly inaccurate for the imaginary part. The real and imaginary parts, however, account for different physical effects and must be considered separately [28, 29]. The inadequacy of the electrostatic expression for the Green's tensor will be illustrated in section 6 using as an example the calculation of the spontaneous emission rate for two interacting molecules near an interface—even when the ratio of the characteristic distances to the free-space wavelength is of the order of $1/300$ and when, according to conventional wisdom, the electrostatic expression should be applicable. We finally note that if antisymmetric electromagnetic resonances (i.e., resonances with zero total dipole moment) can be excited in the system, expansion of the imaginary part of the Green's tensor with the precision $O((\omega/c)^3)$ is not sufficient due to certain cancellations [28, 29]. In this case, higher-order corrections must be used. Excitation of antisymmetric resonances will also be illustrated in section 6.

It follows from the above discussion that obtaining corrections to the electrostatic limiting expression for the Green's tensor is highly desirable. However, despite the fact that it is relatively easy to derive the electrostatic result, it is difficult to obtain corrections to it. These corrections cannot be obtained as a conventional power-series expansion of the Sommerfeld

integrals for the reasons outlined below in section 3. The corrections must be computed at least to third order in $\omega\mathcal{L}/c$. Finally, the expansion must be carried out for all mathematically independent components of the Green's tensor (in the half-space geometry, four components are mathematically independent, while in the more general case, the number of independent components is six). In summary, the required computations are extremely cumbersome and, to the best of our knowledge, have not been published so far.

It may seem that, given the power of modern computers, a satisfactory alternative approach is to avoid the use of any analytical expansions for the Green's tensor and instead compute it by numerical evaluation of the Sommerfeld integrals. The numerical computation of these integrals is not a serious problem *per se*, although a certain degree of care is required, particularly, because the integrals are oscillatory. However, the numerical result is often insufficient or not directly usable. There are many applications, including the near-field inverse scattering problem [9–15], in which knowledge of the analytical dependence of the Green's tensor on the physical parameters of the problem is required. An example that will be explored in some detail below in section 6 is radiative lifetime calculations for interacting molecules without the quasi-particle pole approximation (in the strong interaction regime). In this application, an analytical expression for the frequency-dependent Green's tensor is highly desirable.

In what follows, we construct a short-distance asymptotic expansion for the Green's tensor. The lowest-order term of this expansion corresponds to the electrostatic result that can be otherwise obtained by the method of images. In the case of a general dispersive substrate, we have computed the corrections to third order in the dimensionless length $\omega\epsilon_1\mathcal{L}/c$. Here $\mathcal{L}$ is the length defined in figure 1 below and $\epsilon_1 > 0$ is the permittivity of the upper half-space (assumed to be transparent and dispersionless) in which both the source and the observation point are located. The third-order term contains the first non-vanishing *radiative correction* to the electrostatic expression for the Green's tensor. If both half-spaces are transparent and dispersionless at the frequency of interest, the third-order correction is imaginary and describes a purely radiative process. If, however, one of the half-spaces is absorbing, the third-order correction may have nonzero real part and describes both radiative and non-radiative processes. In the case of a transparent dielectric substrate, we compute the radiative corrections to the imaginary part of the Green's tensor to seventh order. Accounting for these high-order corrections is important since the imaginary part of the Green's tensor is characterized by slower convergence in comparison to the real part. This will be illustrated numerically in sections 5 and 6.

The results obtained are of considerable mathematical complexity. We recognize that coding the formulae of section 4 in a computer program is a very tedious task. Therefore, we have included as supplementary material Fortran-77 codes for computing all the elements of the Green's tensor according to the expansion obtained in this paper. We have also included codes for numerical evaluation of the Sommerfeld integrals.

We note the following conventions which hold throughout this paper. Tensor components in the reference frame shown in figure 1 are denoted by a pair of Greek indices which can take values x, y or z, for instance, $G_{\alpha\beta}$ or G_{xz}. All square roots are uniquely defined by the condition $-\pi/2 < \arg(\sqrt{z}) \leqslant \pi/2$, where z is an arbitrary complex number. Finally, logarithms of complex numbers are defined by the condition $\ln z = \ln|z| + \mathrm{i}\arg(z)$, where $-\pi < \arg(z) \leqslant \pi$.

The remainder of the paper is organized as follows. In section 2, we recall the basic facts about the electromagnetic Green's tensor and its plane-wave representation in the half-space geometry. We then formulate the short-distance expansion in section 3 and present explicit formulae for the radiative corrections through seventh order in section 4. Numerical results

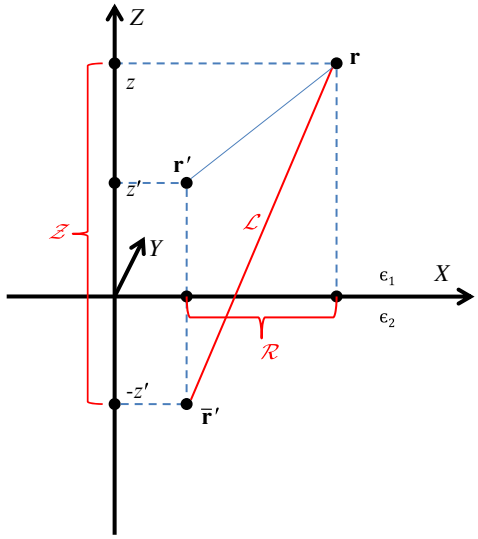

Figure 1. Illustrating the geometry of the problem.

for both metallic and transparent substrates are given in section 5. In section 6, we consider the problem of spontaneous emission by interacting molecules near a substrate and illustrate the utility of the expansion of section 4 with numerical examples. Finally, we summarize and discuss our results in section 7.

2. Theory

By definition, the frequency-domain electromagnetic Green's function $G(\mathbf{r}, \mathbf{r}')$ is a linear operator that gives the complex amplitude of the electric field $\mathbf{E}(\mathbf{r})$ at the point $\mathbf{r}$ due to a point dipole $\mathbf{d}(t) = \mathrm{Re}[\mathbf{d}\exp(-\mathrm{i}\omega t)]$ located at the point $\mathbf{r}'$, according to

$$\mathbf{E}(\mathbf{r}) = G(\mathbf{r}, \mathbf{r}') \cdot \mathbf{d}. \tag{1}$$

The real-valued electric field is obtained as $\mathrm{Re}[\mathbf{E}(\mathbf{r})\exp(-\mathrm{i}\omega t)]$. If the fields are not monochromatic, the electric field may be obtained by Fourier superposition.

We now consider the monochromatic case in the half-space geometry. Let the z-axis of a Cartesian reference frame be perpendicular to the interface. The upper half-space ($z > 0$) is a spatially uniform medium of purely real permittivity ϵ_1 while the lower half-space (the substrate) is a spatially uniform medium of permittivity ϵ_2. The geometry under consideration is illustrated in figure 1. At this point, we do not make any assumptions about ϵ_2. However, some results will be obtained for the special case $\epsilon_2 > 0$, which corresponds to a transparent dielectric.

The Green's tensor satisfies the equation

$$[\nabla_{\mathbf{r}} \times \nabla_{\mathbf{r}} \times -k^2(z)]G(\mathbf{r}, \mathbf{r}') = 4\pi \frac{\omega^2}{c^2}\delta(\mathbf{r} - \mathbf{r}')\mathbb{I}_3, \tag{2}$$

where c is the speed of light in vacuum, $\mathbb{I}_3$ is the unit 3×3 matrix and

$$k^2(z) = \begin{cases} k_1^2, & z > 0 \\ k_2^2, & z < 0 \end{cases} \equiv \left(\frac{\omega}{c}\right)^2 \begin{cases} \epsilon_1, & z > 0 \\ \epsilon_2, & z < 0. \end{cases} \tag{3}$$

In addition to (2), $G(\mathbf{r}, \mathbf{r}')$ satisfies the boundary conditions

$$\hat{\mathbf{z}} \times [G(\mathbf{r}, \mathbf{r}')|_{z=+0} - G(\mathbf{r}, \mathbf{r}')|_{z=-0}] = 0, \tag{4a}$$

$$\hat{\mathbf{z}} \times \nabla \times [G(\mathbf{r}, \mathbf{r}')|_{z=+0} - G(\mathbf{r}, \mathbf{r}')|_{z=-0}] = 0. \tag{4b}$$

In general, the Green's tensor can be written as the sum of two contributions:

$$G(\mathbf{r}, \mathbf{r}') = G^F(\mathbf{r}, \mathbf{r}') + G^R(\mathbf{r}, \mathbf{r}'). \tag{5}$$

Here G^F is the Green's tensor in an infinite homogeneous medium while G^R is the contribution due to the presence of the boundary (the 'reflected' term).

In the case of a planar interface, both contributions to the Green's tensor can be found analytically for arbitrary $\mathbf{r}$ and $\mathbf{r}'$ [2]. We will specialize, however, to the less general case when both points $\mathbf{r}$ and $\mathbf{r}'$ are in the same half-space $z > 0$. This geometry, illustrated in figure 1, is relevant to near-field imaging and many other applications in which both the detector and the source are above the substrate.

The well-known free-space term is given by

$$G^F(\mathbf{r}, \mathbf{r}') = \left(k_1^2 \mathbb{I}_3 + \nabla \otimes \nabla\right) \frac{\exp(\mathrm{i}k_1|\mathbf{r} - \mathbf{r}'|)}{|\mathbf{r} - \mathbf{r}'|}, \tag{6}$$

where $\otimes$ denotes the tensor product. Because of the translational invariance of free space, G^F depends only on $\mathbf{r} - \mathbf{r}'$. This functional dependence can be conveniently written as

$$G^F(\mathbf{r}, \mathbf{r}') = -\frac{4\pi}{3}\delta(\mathbf{r} - \mathbf{r}') + \mathcal{G}^F(\mathbf{r}, \mathbf{r}'), \tag{7}$$

where the singular part $-(4\pi/3)\delta(\mathbf{r} - \mathbf{r}')$ is due to second derivatives of the factor $|\mathbf{r} - \mathbf{r}'|$ in (6) and the regular part, $\mathcal{G}^F(\mathbf{r})$, is given by

$$\mathcal{G}^F(\mathbf{r}) = \left[\left(\frac{k_1^2}{r} + \frac{\mathrm{i}k_1}{r^2} - \frac{1}{r^3}\right)\mathbb{I}_3 + \left(\frac{-k_1^2}{r} + \frac{-3\mathrm{i}k_1}{r^2} + \frac{3}{r^3}\right)\frac{\mathbf{r} \otimes \mathbf{r}}{r^2}\right] \exp(\mathrm{i}k_1 r). \tag{8}$$

Let us expand the functions in (6) in a power series in $k_1 r$. We will write the result separately for the real and the imaginary parts of $\mathcal{G}^F$:

$$\begin{aligned}\mathrm{Re}\,\mathcal{G}^F(\mathbf{r}) = \frac{1}{r^3}\Bigg\{&\left[-1 + \frac{(k_1 r)^2}{2} - \frac{3(k_1 r)^4}{8} + \frac{5(k_1 r)^6}{144} + O((k_1 r)^8)\right]\mathbb{I}_3 \\ &+ \left[3 + \frac{(k_1 r)^2}{2} + \frac{(k_1 r)^4}{8} - \frac{(k_1 r)^6}{48} + O((k_1 r)^8)\right]\frac{\mathbf{r} \otimes \mathbf{r}}{r^2}\Bigg],\end{aligned} \tag{9a}$$

$$\begin{aligned}\mathrm{Im}\,\mathcal{G}^F(\mathbf{r}) = \frac{1}{r^3}\Bigg\{&\left[\frac{2(k_1 r)^3}{3} - \frac{2(k_1 r)^5}{15} + \frac{(k_1 r)^7}{140} + O((k_1 r)^9)\right]\mathbb{I}_3 \\ &+ \left[\frac{(k_1 r)^5}{15} - \frac{(k_1 r)^7}{210} + O((k_1 r)^9)\right]\frac{\mathbf{r} \otimes \mathbf{r}}{r^2}\Bigg\}.\end{aligned} \tag{9b}$$

This formula illustrates and reinforces the physical argument that was made in section 1. Namely, the expansion for $\mathrm{Re}\,\mathcal{G}^F$ starts from the terms which are of the order $r^{-3}O((k_1 r)^0) = O(r^{-3})$ while the expansion for $\mathrm{Im}\,\mathcal{G}^F$ starts from the terms which are of the order $r^{-3}O((k_1 r)^3) = O\left(k_1^3\right)$. We emphasize again that the real and the imaginary parts of the Green's tensor describe different physical effects and must be considered separately. Yet, an expansion similar to (9) for the reflected part of the Green's tensor, $\mathcal{G}^R$, has not been obtained so far. Deriving this expansion is the main goal of this paper.

The reflected part of the Green's tensor can be written in the form of a Fourier integral [2]:

$$G^R(\mathbf{r},\mathbf{r}') = \frac{k_1^2}{2\pi}\int \frac{\mathrm{d}^2 q}{\varkappa_1(q)} D(\mathbf{q}) \exp[i\,\mathbf{q}\cdot(\boldsymbol{\rho}-\boldsymbol{\rho}') - \varkappa_1(q)(z+z')]. \tag{10}$$

In the above equation, $\mathbf{r} = (\boldsymbol{\rho}, z)$ and $\mathbf{r}' = (\boldsymbol{\rho}', z')$, so that $\boldsymbol{\rho}$ is the projection of the vector $\mathbf{r}$ onto the plane $z = 0$, etc, and all other relevant notations are defined below in equations (11)–(15). The operator $D(\mathbf{q})$ can be written as

$$D(\mathbf{q}) = S^{-1}(\mathbf{q}) d(q) S(\mathbf{q}). \tag{11}$$

Here $S(\mathbf{q})$ is the Jacobi rotation matrix whose nonzero components are

$$S_{xx}(\mathbf{q}) = S_{yy}(\mathbf{q}) = q_x/q \equiv \cos(\varphi_{\mathbf{q}}), \tag{12a}$$

$$-S_{yx}(\mathbf{q}) = S_{xy}(\mathbf{q}) = q_y/q \equiv \sin(\varphi_{\mathbf{q}}), \tag{12b}$$

$$S_{zz}(\mathbf{q}) = 1, \tag{12c}$$

with $\varphi_{\mathbf{q}}$ being the angle between the two-dimensional vector $\mathbf{q}$ and the x-axis of the laboratory frame. We note that $[S(\mathbf{q})]\mathbf{q} = q\hat{\mathbf{x}}$. The nonzero components of the tensor $d(q)$ are

$$-d_{xx}(q) = R_2(q)\frac{\varkappa_1^2(q)}{k_1^2}, \tag{13a}$$

$$d_{yy}(q) = R_1(q), \tag{13b}$$

$$-d_{zz}(q) = R_2(q)\frac{q^2}{k_1^2}, \tag{13c}$$

$$d_{xz}(q) = -d_{zx}(q) = R_2(q)\frac{\mathrm{i}q\varkappa_1(q)}{k_1^2}, \tag{13d}$$

where

$$R_1(q) = \frac{\varkappa_1(q) - \varkappa_2(q)}{\varkappa_1(q) + \varkappa_2(q)}, \qquad R_2(q) = \frac{\epsilon_1\varkappa_2(q) - \epsilon_2\varkappa_1(q)}{\epsilon_1\varkappa_2(q) + \epsilon_2\varkappa_1(q)}. \tag{14}$$

Finally, $\varkappa_1(q)$ and $\varkappa_2(q)$ are given by

$$\varkappa_1(q) = \sqrt{q^2 - k_1^2}, \qquad \varkappa_2(q) = \sqrt{q^2 - k_2^2}. \tag{15}$$

We note that while the free-space term $G^F(\mathbf{r},\mathbf{r}')$ depends only on $\mathbf{r}-\mathbf{r}' = (\boldsymbol{\rho}-\boldsymbol{\rho}', z-z')$, the reflected part of the Green's tensor $G^R(\mathbf{r},\mathbf{r}')$ depends on $\boldsymbol{\rho}-\boldsymbol{\rho}'$ and $z+z'$. Let us, for simplicity, choose the x-axis of the laboratory frame so that the projections of both points $\mathbf{r}$ and $\mathbf{r}'$ lie on this axis (see figure 1). In this reference frame, the tensor G^R depends only on the length of the vector $\mathcal{R} = |\rho - \rho'|$ but not on its direction. The functional dependence of the reflected Green's tensor G^R on its arguments can be expressed by writing

$$G^R(\boldsymbol{\rho}, z; \boldsymbol{\rho}', z') = \mathcal{G}^R(|\boldsymbol{\rho}-\boldsymbol{\rho}'|, z+z'), \tag{16}$$

where

$$\mathcal{G}^R(\mathcal{R},\mathcal{Z}) = k_1^2\int_0^\infty \frac{q\,\mathrm{d}q}{\varkappa_1(q)} \exp[-\varkappa_1(q)\mathcal{Z}] F(q,\mathcal{R}) \tag{17}$$

and

$$F(q,\mathcal{R}) = \int_0^{2\pi} \frac{\mathrm{d}\varphi_{\mathbf{q}}}{2\pi} \exp(\mathrm{i}q\mathcal{R}\cos\varphi_{\mathbf{q}}) D(\mathbf{q}). \tag{18}$$

It is important to remember that the variables $\mathcal{Z}$ and $\mathcal{R}$ in (17) are not the physical coordinates of either the source or the point of observation; rather, we have

$$\mathcal{Z} = z + z', \qquad \mathcal{R} = |\boldsymbol{\rho} - \boldsymbol{\rho}'|, \tag{19}$$

so that $\mathcal{Z}$ is the sum of the z-coordinates of the source and the point of observation while $\mathcal{R}$ is the lateral distance between these two points.

The nonzero components of the tensor $F(q, \mathcal{R})$ are

$$F_{xx} = (d_{yy} - d_{xx})\frac{J_1(q\mathcal{R})}{q\mathcal{R}} + d_{xx}J_0(q\mathcal{R}), \tag{20a}$$

$$F_{yy} = (d_{xx} - d_{yy})\frac{J_1(q\mathcal{R})}{q\mathcal{R}} + d_{yy}J_0(q\mathcal{R}), \tag{20b}$$

$$F_{zz} = d_{zz}J_0(q\mathcal{R}), \tag{20c}$$

$$-F_{zx} = F_{xz} = \mathrm{i}d_{xz}J_1(q\mathcal{R}), \tag{20d}$$

where $J_l(x)$ are Bessel functions of the first kind and the components of the tensor $d(q)$ are given in (11).

In what follows, we will use the term 'Green's tensor' for the quantity $\mathcal{G}^R$. Strictly speaking, the Green's tensor must be determined by first computing the reflected part, G^R, according to (16) and then by adding the free space contribution G^F according to (5).

3. Short-distance expansion

In this section, we briefly sketch the derivation of the short-distance expansion. Detailed calculations for one of the matrix elements of $\mathcal{G}^R$ are given in appendices A and B, while the expansions for the other elements can be obtained by direct analogy.

We will assume below that the variables $\mathcal{R}$ and $\mathcal{Z}$ which appear in expression (17) for the Green's tensor are of the same order of magnitude. Mathematically, this is expressed as $\mathcal{R} \sim \mathcal{Z} \sim \mathcal{L}$ where

$$\mathcal{L} = \sqrt{\mathcal{Z}^2 + \mathcal{R}^2} \tag{21}$$

is the characteristic length scale of the problem (see figure 1).

Consider, for example, the tensor element $\mathcal{G}^R_{zz}$. From the formulae of the previous section, we find

$$\mathcal{G}^R_{zz}(\mathcal{R}, \mathcal{Z}) = -\int_0^\infty \frac{q^3 J_0(q\mathcal{R})\,\mathrm{d}q}{\varkappa_1(q)} R_2(q)\exp[-\varkappa_1(q)\mathcal{Z}]. \tag{22}$$

At large values of q, $\varkappa_1(q)$ has a positive real part which is proportional to q, so that the above integral converges at the upper limit exponentially. Suppose now that we expand the Bessel function $J_0(q\mathcal{R})$ into a power series and integrate each term separately. Although each integral in this series converges, it still depends on $\mathcal{Z}$ in a complicated way and the resultant expansion is not useful. If, in addition, we expand the function $\exp[-\varkappa_1(q)\mathcal{Z}]$ in a power series, the integral of each term in the resultant expansion diverges at the upper limit. This is the main difficulty that one encounters in the derivation of the short-distance expansion.

To remedy this situation, we proceed as follows. We first break the integral (22) into two integrals: one from 0 to k_1 and the other from k_1 to infinity. Since the upper half-space is assumed to be transparent, k_1 is a positive constant. Separate consideration of the integrals over the intervals $q \in [0, k_1]$ and $q \in [k_1, \infty)$ is convenient because the function $\kappa_1(q)$ has a branch cut along the ray $q \leqslant k_1$. The integral over the finite interval $[0, k_1]$ does not diverge,

even if the functions $J_0(q\mathcal{R})$ and $\exp[-\varkappa_1(q)\mathcal{Z}]$ are expanded in Taylor series to an arbitrarily high order. As for the second integral, we obtain its short-distance expansion by introducing counter terms. That is, we rewrite the integral (22) as

$$\mathcal{G}^R_{zz}(\mathcal{R},\mathcal{Z}) = -\int_0^{k_1} f(q)J_0(q\mathcal{R})\exp[-\varkappa_1(q)\mathcal{Z}] - \int_{k_1}^{\infty}[f(q)-g(q)]J_0(q\mathcal{R})\exp[-\varkappa_1(q)\mathcal{Z}]\,\mathrm{d}q - \int_{k_1}^{\infty} g(q)J_0(q\mathcal{R})\exp[-\varkappa_1(q)\mathcal{Z}]\,\mathrm{d}q. \tag{23}$$

In the above equation,

$$f(q) = \frac{q^3}{\varkappa_1(q)}R_2(q) = \frac{q^3}{\varkappa_1(q)}\frac{\epsilon_1\varkappa_2(q)-\epsilon_2\varkappa_1(q)}{\epsilon_1\varkappa_2(q)+\epsilon_2\varkappa_1(q)}, \tag{24}$$

while $g(q)$ is an arbitrary function which we require to satisfy the following two conditions:

(i) When $q\to\infty$, $f(q)-g(q) = O(1/q^\alpha)$, where $\alpha > 1$.
(ii) The last integral in (23) must be computable analytically with the same precision as the first two integrals (an explicit example of such calculation is given in appendix A). Therefore, $g(q)$ must be of sufficiently 'simple' form.

The first condition guarantees that, if we expand the factor $\exp[-\varkappa_1(q)\mathcal{Z}]J_0(q\mathcal{R})$ in the second integral in (23) to the order β (the corresponding expansion terms are $\propto(\mathcal{Z}\varkappa_1)^\gamma(\mathcal{R}q)^\delta$, where $\gamma+\delta=\beta$), the resultant integrals will be convergent as long as $\beta < \alpha - 1$.

We have found functions $g(q)$ which satisfy the above conditions with $\alpha = 2$ for all tensor components of $\mathcal{G}^R$. In the case of $\mathcal{G}^R_{zz}$, this function is

$$g(q) = \frac{q^3}{\varkappa_1(q)}\left[s + \frac{s(1-s)k_1^2}{2q^2}\right], \tag{25}$$

where

$$s = (1-\varepsilon)/(1+\varepsilon) \tag{26}$$

and we have introduced the relative permittivity of the two half-spaces, ε, defined by

$$\varepsilon = \epsilon_2/\epsilon_1. \tag{27}$$

Note that the expression in the square brackets in (25) coincides with the first two terms in the expansion of $R_2(q)$ in powers of $1/q$ at large q.

Now, if we replace the factor $\exp[-\varkappa_1(q)\mathcal{Z}]J_0(q\mathcal{R})$ in the first two integrals in (23) by unity, the resultant integrals are $\mathcal{Z}$- and $\mathcal{R}$-independent. At the same time, the third integral contains terms which are of the order of $O(\mathcal{L}^{-3})$, $O(\mathcal{L}^{-2})$, $O(\mathcal{L}^{-1})$ and $O(\mathcal{L}^0)$. We thus conclude that by approximating the factor $\exp[-\varkappa_1(q)\mathcal{Z}]J_0(q\mathcal{R})$ with unity in the first two integrals in (23) and by evaluating the third integral with the precision $O(\mathcal{L}^0)$, we obtain the first four tensor coefficients $\mathcal{K}^{(l)}$ in the expansion

$$\mathcal{G}^R = \mathcal{L}^{-3}\sum_{l=0}^{\infty}(k_1\mathcal{L})^l\mathcal{K}^{(l)}. \tag{28}$$

In what follows, we will refer to the term of order $O(\mathcal{L}^{-3})$ (which correspond to the $l=0$ term in (28) as the zeroth-order term and so forth. The nth-order approximation to $\mathcal{G}^R$ is obtained when all terms with $l \leqslant n$ are accounted for in the above summation. The method described above has allowed us to compute the expansion coefficients in (28) to third order.

The numerical simulations of section 5 show that the imaginary part of $\mathcal{G}^R$ converges with n slower than the real part. As was discussed in section 1, the first nontrivial radiative

correction to $\mathcal{G}^R$ appears only in the third order and even higher-order corrections must be used if antisymmetric electromagnetic modes can be exited in the system. It is therefore desirable to obtain higher-order corrections to $\mathrm{Im}\,\mathcal{G}^R$. We note that $\mathrm{Im}\,\mathcal{G}^R$ is an important physical quantity which is needed, for example, to compute radiative lifetimes of molecules in the vicinity of interfaces [23]. We will provide examples of such computation in the strong interaction regime in section 6.

In principle, it is possible to compute the short-distance expansion to higher orders by using functions $g(q)$ which satisfy the condition (i) with progressively larger values of α, albeit the calculations become very cumbersome for $\alpha > 2$ and are not reported here. However, we have noted that, if ϵ_1 and ϵ_2 are both real, the expansion of $\mathrm{Im}\,\mathcal{G}^R$ can be obtained by more straightforward means. Indeed if the above condition is satisfied, and for $q > (\omega/c)\max(\epsilon_1, \epsilon_2) = \max(k_1, k_2)$, the integrand in (22) is real. Therefore, $\mathrm{Im}\,\mathcal{G}^R$ can be written in this case as an integral over a finite interval. Obviously, the exponent and the Bessel function in this integral can be expanded to arbitrarily high orders without causing the integrals to diverge. By using this idea, we have obtained corrections to $\mathrm{Im}\,\mathcal{G}^R$ up to seventh order. These corrections are applicable to transparent dielectric substrates.

4. Summary of analytical results

The main result of this paper is the expansion (28) which is valid at small distances $\mathcal{R}$ and $\mathcal{Z}$. The small parameter of the theory is $k_1\mathcal{L}$ where $\mathcal{L}$ is defined by (21). In this section, we present expressions for the tensor coefficients $\mathcal{K}^{(l)}$. For a general complex permittivity of the substrate, the expansion (28) is carried to third order. However, for a nonabsorbing substrate with purely real permittivity ϵ_2, we obtain additional terms in the expansion of the *imaginary part* of $\mathcal{G}^R$ up to seventh order. Note that, in all cases, the permittivity ϵ_1 of the upper half-space and, correspondingly, the wave number k_1, are assumed to be real.

It is important to emphasize that the expansion (28) is not a formal power series in $k_1\mathcal{L}$. In particular, the coefficients $\mathcal{K}^{(l)}$ can depend on the frequency, $\mathcal{R}$ and $\mathcal{Z}$. We assume here that this dependence is weak. There are cases, however, when this assumption is manifestly invalid. The most obvious example is the case $\varepsilon \to -1$ which is the condition for a surface resonance. The coefficients in (28) all diverge at $\varepsilon = -1$ and the expansion itself must be used with caution. It should be noted that the same is true for the commonly used electrostatic reflection term which appears as the zeroth-order approximation in our expansion.

4.1. Expansion of the Green's tensor to third order for arbitrary substrates

4.1.1. Zeroth order. The nonzero components of $\mathcal{K}^{(0)}$ are

$$\mathcal{K}^{(0)}_{xx} = \frac{\varepsilon - 1}{\varepsilon + 1}\left[3\left(\frac{\mathcal{Z}}{\mathcal{L}}\right)^2 - 2\right], \tag{29a}$$

$$\mathcal{K}^{(0)}_{yy} = \frac{\varepsilon - 1}{\varepsilon + 1}, \tag{29b}$$

$$\mathcal{K}^{(0)}_{zz} = \frac{\varepsilon - 1}{\varepsilon + 1}\left[3\left(\frac{\mathcal{Z}}{\mathcal{L}}\right)^2 - 1\right], \tag{29c}$$

$$\mathcal{K}^{(0)}_{xz} = \frac{\varepsilon - 1}{\varepsilon + 1}\frac{3\mathcal{Z}\mathcal{R}}{\mathcal{L}^2}. \tag{29d}$$

Note that the above terms can be obtained by the method of images. In figure 1, the point of observation is $\mathbf{r}$ and the point where the source dipole is located is $\mathbf{r}'$. The image (reflected) dipole is located at the point $\bar{\mathbf{r}}'$. The amplitude of the reflected dipole, $\bar{\mathbf{d}}$ is obtained by rotating the amplitude of the original dipole $\mathbf{d}$ by the angle π about the axis connecting the points $\mathbf{r}'$ and $\bar{\mathbf{r}}'$. The reflected part of the Green's tensor is then obtained by acting with the electrostatic limiting expression for the free space Green's tensor G^F on the reflected dipole $\bar{\mathbf{d}}$.

4.1.2. First order. $\mathcal{K}^{(1)}$ is identically zero.

4.1.3. Second order. The nonzero components of $\mathcal{K}^{(2)}$ are

$$\mathcal{K}^{(2)}_{xx} = \frac{\varepsilon-1}{\varepsilon+1}\frac{\mathcal{Z}}{2\mathcal{L}}\left(\frac{\mathcal{Z}}{\mathcal{L}} - \frac{2}{\varepsilon+1}\frac{\mathcal{L}}{\mathcal{L}+\mathcal{Z}}\right), \tag{30a}$$

$$\mathcal{K}^{(2)}_{yy} = \frac{\varepsilon-1}{2(\varepsilon+1)}\left(\frac{\varepsilon-1}{\varepsilon+1}\frac{\mathcal{L}}{\mathcal{L}+\mathcal{Z}} + \frac{\mathcal{Z}}{\mathcal{L}+\mathcal{Z}}\right), \tag{30b}$$

$$\mathcal{K}^{(2)}_{zz} = \frac{\varepsilon-1}{2(\varepsilon+1)}\left[\left(\frac{\mathcal{Z}}{\mathcal{L}}\right)^2 + \frac{3\varepsilon+1}{\varepsilon+1}\right], \tag{30c}$$

$$\mathcal{K}^{(2)}_{xz} = \frac{\varepsilon-1}{\varepsilon+1}\sqrt{\frac{\mathcal{L}-\mathcal{Z}}{\mathcal{L}+\mathcal{Z}}}\left[\frac{\varepsilon}{\varepsilon+1} + \frac{\mathcal{Z}}{2\mathcal{L}}\left(1+\frac{\mathcal{Z}}{\mathcal{L}}\right)\right]. \tag{30d}$$

4.1.4. Third order. The tensor $\mathcal{K}^{(3)}$ does not depend on the spatial variables $\mathcal{R}$ and $\mathcal{Z}$ and its only nonzero components are

$$\mathcal{K}^{(3)}_{xx} = \mathcal{K}^{(3)}_{yy} = \frac{\mathrm{i}\varepsilon}{(\varepsilon+1)^2}\left[\frac{1-3\sqrt{\varepsilon}+3\varepsilon+2\varepsilon^2}{3(\sqrt{\varepsilon}+1)} + \Lambda(\varepsilon)\right] \tag{31a}$$

$$\mathcal{K}^{(3)}_{zz} = -\frac{2\mathrm{i}}{(\varepsilon+1)^2}\left[\frac{1+\sqrt{\varepsilon}+2\varepsilon+2\varepsilon^{3/2}-2\varepsilon^{5/2}-\varepsilon^3}{3(\sqrt{\varepsilon}+1)} + \varepsilon^2\Lambda(\varepsilon)\right], \tag{31b}$$

where

$$\Lambda(\varepsilon) = \frac{\varepsilon}{(\varepsilon-1)\sqrt{\varepsilon+1}}\ln\frac{1+\sqrt{\varepsilon+1}}{\varepsilon+\sqrt{\varepsilon}\sqrt{\varepsilon+1}}. \tag{32}$$

Note that $\mathcal{K}^{(3)}_{xz} = 0$.

Formulae (31) are regular when $\varepsilon \to 1$. In particular, the following expansions can be obtained:

$$\mathcal{K}^{(3)}_{xx} = \frac{\mathrm{i}}{6}(\varepsilon-1) + \frac{\mathrm{i}}{12}(\varepsilon-1)^2 + O((\varepsilon-1)^3), \tag{33a}$$

$$\mathcal{K}^{(3)}_{zz} = \frac{5\mathrm{i}}{6}(\varepsilon-1) - \frac{\mathrm{i}}{12}(\varepsilon-1)^2 + O((\varepsilon-1)^3). \tag{33b}$$

4.2. Corrections to the imaginary part of the Green's tensor to seventh order for transparent substrates

Expressions for $\operatorname{Im}\mathcal{K}^{(l)}$ up to seventh order are given below for purely real, positive permittivities ϵ_1 and ϵ_2. Correspondingly, in all formulae of this section, the relative

permittivity $\varepsilon = \epsilon_2/\epsilon_1$ must be viewed as a positive real variable. At even orders, the results will be expressed through certain rational functions $r_k(\sqrt{\varepsilon})$ of the relative refractive index and the logarithmic function of the relative permittivity, $\Lambda(\varepsilon)$, which is defined in (32). At odd orders, the results will be expressed in terms of polynomials $p_k(\varepsilon)$. The functions $r_k(x)$ and $p_k(x)$ are given in appendix C.

Note that the expansion coefficients obtained in this subsection cannot be analytically continued to complex or negative frequencies. Indeed, by making the assumption that ε is real, we have violated the fundamental symmetry property $\varepsilon(-\omega) = \varepsilon^*(\omega)$ which is characteristic of any linear response and of the Green's tensor in particular. If the calculations are carried out for complex ε with infinitesimally small imaginary part, it can be shown that the expansion coefficients of the fourth- and six-order terms must be multiplied by the factor $\mathrm{sgn}[\mathrm{Im}\,\varepsilon(\omega)] = \mathrm{sgn}(\omega)$ and therefore are not analytic functions of either ε or ω. This factor is omitted below for simplicity.

4.2.1. Fourth order.

$$\mathrm{Im}\,\mathcal{K}^{(4)}_{yy} = \mathrm{Im}\,\mathcal{K}^{(4)}_{xx} = -\frac{\mathcal{Z}}{\mathcal{L}}\frac{\pi}{16}\frac{\varepsilon-1}{(\varepsilon+1)^3}p_1(\varepsilon), \tag{34a}$$

$$\mathrm{Im}\,\mathcal{K}^{(4)}_{zz} = -\frac{\mathcal{Z}}{\mathcal{L}}\frac{\pi}{8}\frac{\varepsilon(\varepsilon-1)}{(\varepsilon+1)^3}p_2(\varepsilon), \tag{34b}$$

$$\mathrm{Im}\,\mathcal{K}^{(4)}_{xz} = \frac{\mathcal{R}}{\mathcal{L}}\frac{\pi}{16}\frac{\varepsilon(\varepsilon-1)}{(\varepsilon+1)^3}p_2(\varepsilon). \tag{34c}$$

4.2.2. Fifth order.

$$\mathrm{Im}\,\mathcal{K}^{(5)}_{xx} = \frac{1}{120(1+\varepsilon)^3}\left\{\frac{4\mathcal{Z}^2}{\mathcal{L}^2}[r_1(\sqrt{\varepsilon}) - 15\varepsilon\Lambda(\varepsilon)] - \frac{\mathcal{R}^2}{\mathcal{L}^2}[r_2(\sqrt{\varepsilon}) + 45\varepsilon^2\Lambda(\varepsilon)]\right\}, \tag{35a}$$

$$\mathrm{Im}\,\mathcal{K}^{(5)}_{yy} = \frac{1}{120(1+\varepsilon)^3}\left\{\frac{4\mathcal{Z}^2}{\mathcal{L}^2}[r_1(\sqrt{\varepsilon}) - 15\varepsilon\Lambda(\varepsilon)] - \frac{\mathcal{R}^2}{\mathcal{L}^2}[r_3(\sqrt{\varepsilon}) + 15\varepsilon^2\Lambda(\varepsilon)]\right\}, \tag{35b}$$

$$\mathrm{Im}\,\mathcal{K}^{(5)}_{zz} = \frac{1}{30(1+\varepsilon)^3}\left\{\frac{2\mathcal{Z}^2}{\mathcal{L}^2}[r_4(\sqrt{\varepsilon}) + 15\varepsilon^2\Lambda(\varepsilon)] - \frac{\mathcal{R}^2}{\mathcal{L}^2}[r_5(\sqrt{\varepsilon}) - 15\varepsilon^3\Lambda(\varepsilon)]\right\}, \tag{35c}$$

$$\mathrm{Im}\,\mathcal{K}^{(5)}_{xz} = -\frac{1}{15(1+\varepsilon)^3}\frac{\mathcal{Z}\mathcal{R}}{\mathcal{L}^2}[r_4(\sqrt{\varepsilon}) + 15\varepsilon^2\Lambda(\varepsilon)]. \tag{35d}$$

4.2.3. Sixth order.

$$\mathrm{Im}\,\mathcal{K}^{(6)}_{xx} = \frac{\pi(\varepsilon-1)}{64(\varepsilon+1)^4}\left\{-\frac{\mathcal{Z}^3}{3\mathcal{L}^3}p_3(\varepsilon) + \frac{\mathcal{Z}\mathcal{R}^2}{4\mathcal{L}^3}p_4(\varepsilon)\right\}, \tag{36a}$$

$$\mathrm{Im}\,\mathcal{K}^{(6)}_{yy} = \frac{\pi(\varepsilon-1)}{64(\varepsilon+1)^4}\left\{-\frac{\mathcal{Z}^3}{3\mathcal{L}^3}p_3(\varepsilon) + \frac{\mathcal{Z}\mathcal{R}^2}{4\mathcal{L}^3}p_5(\varepsilon)\right\}, \tag{36b}$$

$$\mathrm{Im}\,\mathcal{K}^{(6)}_{zz} = \frac{\pi\varepsilon(\varepsilon-1)}{32(\varepsilon+1)^4}\left\{-\frac{\mathcal{Z}^3}{3\mathcal{L}^3}p_6(\varepsilon) + \frac{\mathcal{Z}\mathcal{R}^2}{2\mathcal{L}^3}p_7(\varepsilon)\right\}, \tag{36c}$$

$$\operatorname{Im}\mathcal{K}_{xz}^{(6)} = \frac{\pi\varepsilon(\varepsilon-1)}{64(\varepsilon+1)^4}\left\{\frac{\mathcal{R}\mathcal{Z}^2}{\mathcal{L}^3}p_6(\varepsilon) - \frac{\mathcal{R}^3}{4\mathcal{L}^3}p_7(\varepsilon)\right\}. \tag{36d}$$

4.2.4. Seventh order.

$$\operatorname{Im}\mathcal{K}_{xx}^{(7)} = \frac{1}{20160(\varepsilon+1)^4}\left\{\frac{8\mathcal{Z}^4}{\mathcal{L}^4}[r_6(\sqrt{\varepsilon}) + 105\varepsilon\Lambda(\varepsilon)] + \frac{12\mathcal{Z}^2\mathcal{R}^2}{\mathcal{L}^4}[-r_7(\sqrt{\varepsilon}) + 315\varepsilon^2\Lambda(\varepsilon)] + \frac{\mathcal{R}^4}{\mathcal{L}^4}[r_8(\sqrt{\varepsilon}) + 525\varepsilon^3\Lambda(\varepsilon)]\right\}, \tag{37a}$$

$$\operatorname{Im}\mathcal{K}_{yy}^{(7)} = \frac{1}{20160(\varepsilon+1)^4}\left\{\frac{8\mathcal{Z}^4}{\mathcal{L}^4}[r_6(\sqrt{\varepsilon}) + 105\varepsilon\Lambda(\varepsilon)] + \frac{12\mathcal{Z}^2\mathcal{R}^2}{\mathcal{L}^4}[-r_9(\sqrt{\varepsilon}) + 105\varepsilon^2\Lambda(\varepsilon)] + \frac{\mathcal{R}^4}{\mathcal{L}^4}[r_{10}(\sqrt{\varepsilon}) + 105\varepsilon^3\Lambda(\varepsilon)]\right\}, \tag{37b}$$

$$\operatorname{Im}\mathcal{K}_{zz}^{(7)} = \frac{1}{3360(\varepsilon+1)^4}\left\{\frac{8\mathcal{Z}^4}{3\mathcal{L}^4}[r_{11}(\sqrt{\varepsilon}) - 105\varepsilon^2\Lambda(\varepsilon)] - \frac{8\mathcal{Z}^2\mathcal{R}^2}{\mathcal{L}^4}[r_{12}(\sqrt{\varepsilon}) + 105\varepsilon^3\Lambda(\varepsilon)] + \frac{\mathcal{R}^4}{\mathcal{L}^4}[r_{13}(\sqrt{\varepsilon}) - 105\varepsilon^4\Lambda(\varepsilon))]\right\}, \tag{37c}$$

$$\operatorname{Im}\mathcal{K}_{xz}^{(7)} = \frac{1}{840(\varepsilon+1)^4}\left\{-\frac{4\mathcal{Z}^3\mathcal{R}}{3\mathcal{L}^4}[r_{11}(\sqrt{\varepsilon}) - 105\varepsilon^2\Lambda(\varepsilon)] + \frac{\mathcal{Z}\mathcal{R}^3}{\mathcal{L}^4}[r_{12}(\sqrt{\varepsilon}) + 105\varepsilon^3\Lambda(\varepsilon)]\right\}. \tag{37d}$$

5. Numerical examples: computation of the Green's tensor

In this section, we illustrate the short-distance expansion of the Green's tensor with numerical examples. We will compare the approximate analytical formulae of section 4 to the results of numerical computation of the Green's tensor. For numerical computation, the necessary integrals were evaluated by Simpson's fifth-order method. In a number of cases, results were verified by numerical integration using the trapezoidal rule. The two numerical integration methods yielded nearly identical results.

In all simulations we assume that the upper half-space is vacuum so that $k_1 = k = \omega/c$.

5.1. Metallic substrate

We start with the more difficult case of a metallic substrate. More specifically, we have assumed that the substrate is made of silver whose permittivity was taken to be

$$\epsilon_2 = \epsilon_0 - \frac{\omega_p^2}{\omega(\omega + \mathrm{i}\gamma)}. \tag{38}$$

In the above expression, $\epsilon_0 \approx 5$ is a term due to interzone transitions, ω_p is the plasma frequency and γ is the Drude relaxation constant. In the case of silver, the vacuum wavelength at the plasma frequency is $\lambda_p = 2\pi c/\omega_p \approx 136$ nm and $\gamma/\omega_p \approx 0.002$. The permittivity of the upper half-space was assumed to be unity ($\epsilon_1 = 1$). Since, in the case of a metallic substrate, $\varepsilon = \epsilon_2/\epsilon_1$ is complex, we have used the analytical expansion of the Green's tensor

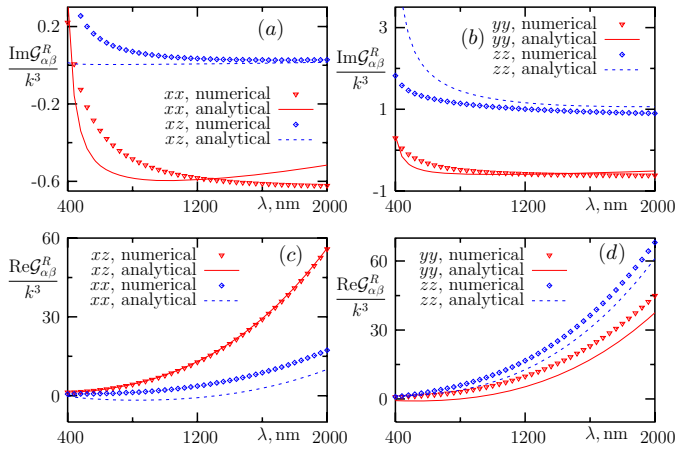

Figure 2. Imaginary (a) and (b) and real (c) and (d) parts of the Green's tensor $\mathcal{G}^R$ for a silver substrate as functions of the wavelength λ for $\mathcal{R} = 40$ nm and $\mathcal{Z} = 80$ nm. The tensor components shown are xx, xz (a) and (c) and yy, zz (b) and (d). Analytical results computed to the third order of the expansion (28) are shown by lines and numerical results by centered symbols.

to third order (the respective formulae are given in section 4.1. We note that the silver substrate is, perhaps, the most stringent test of the short-distance expansion.

The results are shown in figure 2. It can be seen that there is a reasonably good correspondence between the numerically and analytically calculated Green's tensor when $\mathcal{R} = 40$ nm and $\mathcal{Z} = 80$ nm. The reader should recall variable $\mathcal{Z}$ in the expression $\mathcal{G}^R(\mathcal{R}, \mathcal{Z})$ is the sum of z-coordinates of the source and the observation point. The spatial arguments of the Green's tensor used in figure 2 may correspond to the points $\mathbf{r}$ and $\mathbf{r}'$ being separated by a horizontal distance of 40 nm with both 40 nm above the interface, for example. For larger distances, the accuracy deteriorates and when $\mathcal{R} = 80$ nm and $\mathcal{Z} = 160$ nm, the difference between the numerical and analytical results is large (data not shown). The accuracy, however, quickly improves for shorter distances. This is illustrated in figure 3(a) where we plot the absolute difference between the analytical and the numerical results for $\mathcal{G}^R_{xx}(\mathcal{R}, \mathcal{Z})$, computed for $\mathcal{R} = \mathcal{Z}/2$ and various values of $\mathcal{Z}$. It can be seen that the error of the analytical approximation decreases when the distances are decreased. This is especially evident for smaller wavelengths, e.g., $\lambda < 1200$ nm.

Note that in the spectral range and for the geometrical parameters used in figure 2, the imaginary part of the Green's tensor is dominated by the first non-vanishing radiative correction which is given by the third-order term (see formulae in section 4.1.4). Since the coefficient $\mathcal{K}^{(3)}_{xz}$ is identically zero, the imaginary part of the corresponding component of the Green's tensor is small, as can be seen in figure 2(a).

Until this point, we have computed the Green's tensor in the spectral interval from the visible to the infrared. However, one may expect that the short distance expansion should become increasingly accurate at sufficiently large values of the wavelength for fixed $\mathcal{R}$ and $\mathcal{Z}$. This behavior was not demonstrated in figure 2. The reason is that we did not consider sufficiently large wavelengths. To illustrate this point, we plot in figure 3(b) $\mathrm{Im}\,\mathcal{G}^R_{zz}(\mathcal{R}, \mathcal{Z})$ as a function of wavelength (for fixed values of $\mathcal{R}$ and $\mathcal{Z}$) up to $\lambda = 1$cm. In this figure, we plot the analytical results computed to various orders of approximation n.

It can be seen that at very large wavelengths, all three approximations ($n = 0$, $n = 2$ and $n = 3$) and the numerical curve coincide. At smaller wavelengths (i.e., $\lambda \lesssim 10\,\mu$m), however,

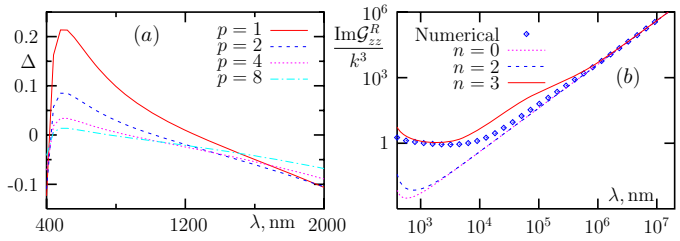

Figure 3. (*a*) Discrepancy Δ between the quantity $\mathrm{Im}\mathcal{G}^R_{xx}$ computed numerically and analytically for a silver substrate computed for $\mathcal{R} = \mathcal{Z}/2 = 40\ \mathrm{nm}p^{-1}$, where p is a positive integer varying from 1 to 8, as labeled. (*b*) Imaginary part of the Green's tensor element $\mathcal{G}^R_{zz}$ for a silver substrate computed for $\mathcal{R} = 40$ nm and $\mathcal{Z} = 80$ nm as a function of the wavelength in the spectral interval from the visible to centimeter waves. The variable n indicates the level of analytical approximation. The nth order result accounts for all terms in (28) with $l \leqslant 3$.

the $n = 3$ curve provides a reasonably accurate approximation while the electrostatic result ($n = 0$) and the first non-vanishing correction to the latter ($n = 2$) deviate from the numerical results by the factor of $\sim$100. In this spectral region, the imaginary part of the Green's tensor is dominated by radiative effects which are not captured in the electrostatic limit.

For the case $n = 3$, there are two distinct spectral regions where the agreement of the analytical and numerical results is quite good. The first region is centered around $\lambda = 1\,\mu$m and the other region corresponds to $\lambda \gtrsim 1$ mm. We can understand this result qualitatively if we consider the physical condition under which the method of images (the zeroth-order approximation or the electrostatic result in our terminology) is valid. This condition is $\mathcal{Z} \ll \delta$ where δ is the skin layer depth. In the Drude model which was adopted in this section, the skin layer depth is, approximately, $\delta \sim c/\gamma \approx 10\,\mu$m if $\omega \approx \omega_p$, $\delta \approx c/\omega_p \approx 20$ nm if $\gamma \ll \omega \ll \omega_p$ and $\delta \approx (c/\omega_p)\sqrt{2\gamma/\omega}$ if $\omega \ll \gamma$. Thus, the short distance expansion can be expected to be valid when $\gamma \ll \omega \ll \omega_p$ (this is the spectral region around $\lambda = 1\,\mu$m) and also when $\omega \ll \gamma$ (this is the region $\lambda \gtrsim 1$ mm). It is interesting to note, however, that for $\lambda \sim 0.1$ mm, the electrostatic curve $n = 0$ provides a better approximation than the $n = 3$ curve. We are not sure whether this is a mere coincidence or a systematic effect.

5.2. *Transparent substrate*

We now turn to the case of a dielectric substrate. We will assume that the substrate is a transparent glass of permittivity $\epsilon_2 = 2.5$ which is independent of frequency in the spectral interval of interest. In numerical simulations shown in this subsection, a small imaginary part equal to $\mathrm{i}10^{-4}$ has been added to ϵ_2. This is needed to regularize the mathematical expressions of section 4.1. However, the results are practically independent of the magnitude of the imaginary part and would be numerically indistinguishable if we chose, for example, $\mathrm{Im}\,\epsilon_2 = 10^{-8}$.

We will compute the analytical approximation to the real part of the Green's tensor to third order according to the formulae of section 4.1. The imaginary part will be computed to seventh order using the corrections of section 4.2. We note that the formulae for these higher-order corrections contain only the real part of ϵ_2, while the imaginary part of ϵ_2 is assumed to be positive and infinitesimally small.

We begin by considering the same geometry as was used in figure 2. The results are shown in figure 4. It can be seen that the correspondence between the analytical and numerical results is very close. We next increase the value of $\mathcal{Z}$ to 160 nm (figure 5). The quality of

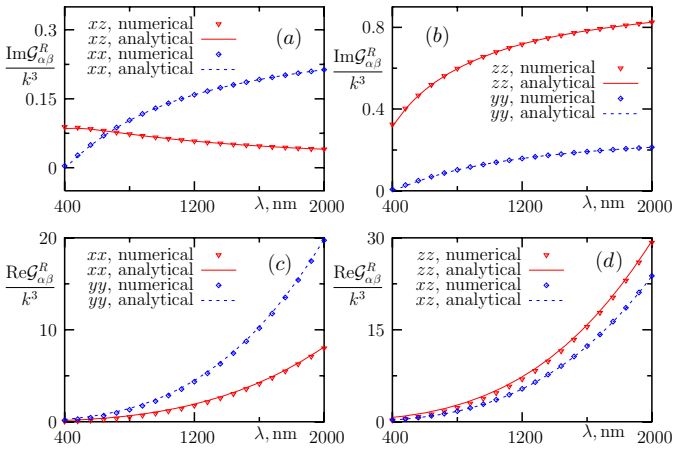

Figure 4. Same as in figure 2 but for a transparent substrate with $\epsilon_2 = 2.5$.

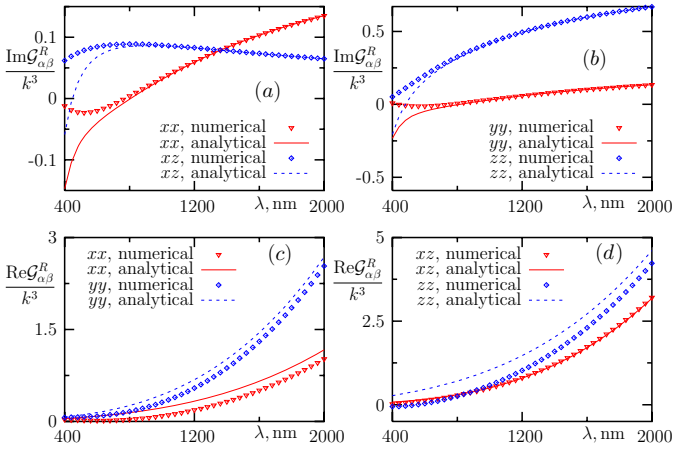

Figure 5. Same as in figure 4 but for $\mathcal{Z} = 160$ nm.

the analytical approximation is now not as good as for $\mathcal{Z} = 80$ nm, yet it is still reasonable, especially at larger wavelengths. We note that, for the imaginary parts of the Green's tensor, the accuracy is excellent for $\lambda > 800$ nm. However, the analytical and numerical results for the real part noticeably deviate from each other even at $\lambda = 2000$ nm. This is explained by fact that the imaginary part was computed to seventh order but the real part only to third order. To illustrate the importance of the higher-order corrections, we plot in figure 6 $\mathrm{Im}\,\mathcal{G}^R_{xx}(\mathcal{R}, \mathcal{Z})$ for the same parameters as in figure 5 but for different orders of approximation. It can be seen that the effect of including the higher-order corrections can be quite dramatic, especially at smaller wavelengths.

6. Application: computation of the spontaneous emission rate

In this section, we illustrate the use of the analytical results derived above with a simple physical example. Specifically, we will compute the spontaneous emission rate for two

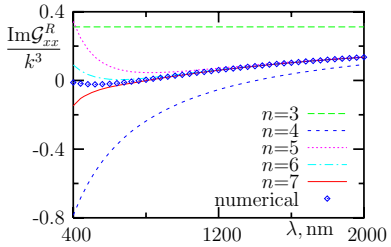

Figure 6. Analytical approximation to $\mathrm{Im}\,\mathcal{G}^R_{xx}$ of different orders and convergence to the numerical result. Parameters are same as in figure 5. The variable n indicates the level of analytical approximation. The nth-order result accounts for all terms in (28) with $l \leqslant 3$.

interacting molecules near an interface. Traditionally, computations of this kind are carried out in the so-called quasi-particle pole approximation. In this approximation, the Green's tensor must be evaluated only at a known fixed frequency. However, in the strong interaction limit, the quasi-particle pole approximation may not be accurate. If this is, indeed, the case, the spontaneous emission rate must be computed by finding the natural frequencies of the system from the characteristic equation. In the latter approach, the Green's tensor appears in a transcendental equation which must be solved with respect to the complex frequency. For this purpose, numerical evaluation of the Green's tensor is obviously inadequate. The results of this paper, however, can be used directly and efficiently.

We now describe a simple classical model for a two-level molecule. The molecule is assumed to be sufficiently small so that it radiates as an electric dipole. The electric quadrupole, magnetic dipole and all other higher-order multipole contributions to the radiation field are neglected. Accordingly, the molecule can be characterized by a linear dipole polarizability $\alpha(\omega)$ which is of the form

$$\alpha(\omega) = V \frac{\omega_0^2}{\omega_0^2 - \omega^2 - \Sigma_0(\omega)}. \tag{39}$$

Here V is a constant of the dimensionality of volume ($V \sim R^3$, where R is the molecular radius), ω_0 is the transition frequency and $\Sigma_0(\omega)$ is the self-energy which describes interaction of the molecule with its own radiation field. In principle, $\Sigma_0(\omega)$ can include other relaxation processes and, in particular, nonradiative relaxation. However, we assume here that the only available relaxation channel for the molecule in free space is spontaneous emission. In this case, the self-energy can be determined from the simple condition that the scattering and extinction cross sections of the molecule are equal for all incident frequencies and there are, therefore, no non-radiative losses [28]. This condition is $4\pi k\,\mathrm{Im}\,\alpha(\omega) = (8\pi/3)k^4|\alpha(\omega)|^2$ where $k = \omega/c$. In this section, similarly to section 5, we assume that the upper half-space is vacuum so that $k_1 = k$. From the above condition, we find that

$$\Sigma_0(\omega) = \mathrm{i}\beta\omega_0^2(\omega/\omega_0)^3, \tag{40}$$

where

$$\beta = (2/3)(\omega_0/c)^3 V = (2/3)k_0^3 V \ll 1 \tag{41}$$

is a small coupling constant.

Now, if an external electric field $\mathbf{E}_0 \exp(-\mathrm{i}\omega t)$ is applied to the molecule, the complex amplitude $\mathbf{d}$ of the dipole moment is found from $\alpha^{-1}(\omega)\,\mathbf{d} = \mathbf{E}_0$. The characteristic equation is

obtained by setting $\mathbf{E}_0 = 0$ and seeking the condition under which the equation $\alpha^{-1}(\omega)\,\mathbf{d} = 0$ has a non-trivial solution. This condition is $\alpha^{-1}(\omega) = 0$ or, equivalently,

$$\omega^2 = \omega_0^2 - \Sigma_0(\omega). \tag{42}$$

Substituting expression (40) for the self-energy into (42), we obtain the cubic equation

$$(\omega/\omega_0)^2 = 1 - \mathrm{i}\beta(\omega/\omega_0)^3. \tag{43}$$

In the limit $\beta \to 0$, the three roots of this equation are

$$\omega_1 = \omega_0(1 - \mathrm{i}\beta/2 - 5\beta^2/8 + \cdots), \tag{44a}$$

$$\omega_2 = \omega_0(-1 - \mathrm{i}\beta/2 + 5\beta^2/8 + \cdots), \tag{44b}$$

$$\omega_3 = \mathrm{i}\omega_0 \frac{1+\beta^2}{\beta} + \cdots. \tag{44c}$$

The third root is unphysical since it is located in the upper complex half-plane and, therefore, violates causality. However, this violation is insignificant since the time advance (by which an effect can precede its cause if we take this root into account) is proportional to β/ω_0 and is, therefore, small in the limit $\beta \to 0$. The unphysical root can be completely removed by using a more accurate expression for the self-energy $\Sigma_0(\omega)$ with frequency-dependent real-valued corrections [30, 31]. These corrections are ignored here for simplicity and the unphysical root ω_3 will also be ignored.

The two remaining roots, ω_1 and ω_2, correctly describe the dynamics of the dipole moment after excitation by a short pulse. The relaxation rate for an isolated molecule is found to the first non-vanishing order in β as

$$\Gamma_0 = -\mathrm{Im}\,\omega_1 = \omega_0[\beta/2 + O(\beta^3)]. \tag{45}$$

The same result for Γ_0 can be obtained by using the quasi-particle pole approximation. The approximation is obtained by iterating equation (43) once starting from $\omega/\omega_0 = 1$ and expanding the square root. Thus, in the quasi-particle pole approximation, the self-energy is evaluated at the transition frequency ω_0. Note that a conceptually similar approximation is used in the quantum theory of spontaneous emission (the Weisskopf–Wigner theory [32]).

We now generalize the problem and consider two identical electromagnetically interacting molecules located at points $\mathbf{r}_a$ and $\mathbf{r}_b$ above a substrate. The characteristic equation in this case reads

$$\alpha^{-1}(\omega)\,\mathbf{d}_a = G^R(\mathbf{r}_a, \mathbf{r}_a; \omega)\,\mathbf{d}_a + G(\mathbf{r}_a, \mathbf{r}_b; \omega)\,\mathbf{d}_b, \tag{46a}$$

$$\alpha^{-1}(\omega)\,\mathbf{d}_b = G(\mathbf{r}_b, \mathbf{r}_a; \omega)\,\mathbf{d}_a + G^R(\mathbf{r}_b, \mathbf{r}_b; \omega)\,\mathbf{d}_b, \tag{46b}$$

where we have explicitly indicated the dependence of the Green's tensor on the frequency. The terms $G^R(\mathbf{r}_a, \mathbf{r}_a; \omega)\,\mathbf{d}_a$ and $G^R(\mathbf{r}_b, \mathbf{r}_b; \omega)\,\mathbf{d}_b$ describe interaction of the molecules with the substrate. It is important to note that only the reflected part of the Green's tensor, G^R, appears in these two expressions. The terms $G(\mathbf{r}_a, \mathbf{r}_b; \omega)\,\mathbf{d}_b$ and $G(\mathbf{r}_b, \mathbf{r}_a; \omega)\,\mathbf{d}_a$ describe the dipole–dipole interaction of the molecules. Here, the full Green's tensor, $G = G^F + G^R$, must be used. Equations (46) have a non-trivial solution provided that

$$\det\left[(\omega_0^2 - \omega^2)\mathbb{I}_6 - \Sigma(\omega)\right] = 0, \tag{47}$$

where $\Sigma(\omega)$ is now a 6×6 matrix defined by

$$\Sigma(\omega) = \Sigma_0(\omega)\mathbb{I}_6 + \omega_0^2 V W(\omega), \tag{48}$$

where $\mathbb{I}_6$ is the 6×6 unit matrix and the interaction operator $W(\omega)$ is given by

$$W(\omega) = \begin{pmatrix} G^R(\mathbf{r}_a, \mathbf{r}_a; \omega) & G(\mathbf{r}_a, \mathbf{r}_b; \omega) \\ G(\mathbf{r}_b, \mathbf{r}_a; \omega) & G^R(\mathbf{r}_b, \mathbf{r}_b; \omega) \end{pmatrix}. \tag{49}$$

The quasi-particle pole approximation is obtained as above by evaluating the self-energy $\Sigma(\omega)$ at the transition frequency ω_0. The matrix $W(\omega)$ has six eigenvalues $w_k(\omega)$ and six eigenvectors $v_k(\omega)$, where $k = 1, \ldots, 6$ labels the oscillation modes. Since W is complex symmetric and, hence, non-Hermitian, its eigenvalues are also complex. Normalization of the eigenvectors can always be chosen so that $v_k \cdot v_l = \delta_{kl}$ where, instead of the scalar product, we have used the dot product (without the use of complex conjugation) of the six-dimensional vectors v_k and v_l [29, 33]. The spontaneous emission rate for the kth mode, Γ_k, is then given in the quasi-particle pole approximation by

$$\frac{\Gamma_k}{\Gamma_0} = \frac{\mathrm{Im}[v_k \cdot \Sigma(\omega_0) v_k]}{\mathrm{Im}[\Sigma_0(\omega_0)]} = 1 + V\omega_0^2 \frac{\mathrm{Im}[w_k(\omega_0)]}{\mathrm{Im}[\Sigma_0(\omega_0)]} = 1 + \frac{\mathrm{Im}[w_k(\omega_0)]}{2k_0^3/3}. \tag{50}$$

An alternative, more accurate approach, is to seek complex natural frequencies as roots of (47). Obviously, the use of the integral representation (10) for the Green's tensor in this approach is very problematic. Even if an iterative root-finding algorithm is adopted, the Green's tensor must be evaluated by numerical integration at each iteration step for complex values of the frequency, when numerical convergence of the integral cannot be guaranteed.

The problem is greatly simplified by using the analytical expansion for the Green's tensor derived in this paper (28). It can be seen that in this case (47) is a transcendental equation of the form $F(\omega) = 0$. It is important that the function $F(\omega)$ is known in terms of elementary functions. Therefore, standard root-finding algorithms such as Newton's method can be easily applied. An additional simplification is obtained in the case of a dielectric dispersionless substrate which we consider in this section. It can be seen that in this case all the transcendental functions that appear in the formulae of section 4 for the expansion coefficients $\mathcal{K}^{(l)}$ become frequency-independent. If, in addition, we also expand the free-space Green's tensor $G^F(\mathbf{r}_a, \mathbf{r}_b; \omega)$ to a finite order in $k\mathcal{L}$, the equation for natural frequencies becomes algebraic. In numerical simulations, we have expanded $G^F(\mathbf{r}_a, \mathbf{r}_b; \omega)$ to seventh order according to (9) which is more than sufficient for convergence.

Further, for the case of two molecules, the matrices $W(\omega)$ and $\Sigma(\omega)$ are block diagonal and the modes polarized in the XZ-plane and along the Y-axis can be considered separately. For the XZ-polarization, the maximum order of the characteristic equation is 28 while for the Y-polarization the maximum order is 14 (the maximum order is obtained when the seventh-order corrections given in section 4.2 to the Green's tensor are taken into account). In the simulations reported below, we have used the method of diagonalization of the companion matrix [34] to find the roots. This method is very stable numerically.

After the complex roots of (47) are found, they must be sorted. Most of the roots have very large imaginary parts which correspond to oscillatory modes with very short lifetimes. These modes are experimentally unobservable and can be ignored. Note that some of these short-lived modes may be unphysical due to the imprecise definition of $\Sigma_0(\omega)$, as is discussed above for the case of an isolated molecule. Numerically, we have found that the six roots with positive real parts and the smallest absolute values of the imaginary parts are well separated from the rest of the roots in the complex plane and are all physical, i.e., have negative imaginary parts. The radiative relaxation rate of the kth mode is obtained as $\Gamma_k = -\mathrm{Im}\,\omega_k$, similar to (45).

In what follows, we will compare the results for Γ_k/Γ_0 obtained in the quasi-particle pole approximation and by solving the dispersion equation (47). We will also compare the results

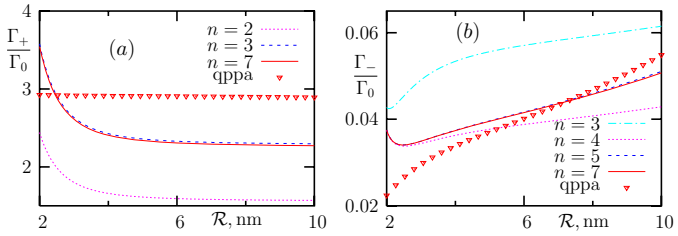

Figure 7. Normalized spontaneous decay rate as a function of the intermolecular distance $\mathcal{R}$ for the symmetric (a) and the antisymmetric (b) oscillation mode computed in the quasi-particle pole approximation (centered symbols, labeled as 'qppa') and by solving the dispersion equation (47) in which the analytical expansion (28) for the reflected part of the Green's tensor has been used (lines) to various orders n, as labeled. The free-space contribution to the Green's tensor, G^F was expanded to seventh order in all cases. The upper half-space is vacuum. Both molecules are situated 1 nm above a dispersionless glassy substrate of permittivity $\epsilon_2 = 2.5$. Other parameters: $\omega_0 = 2\pi c/300$ nm (c: speed of light in vacuum) and $V = (4\pi/3)(1\text{ nm})^3$.

obtained by using the analytical expansion (28) for the Green's tensor computed to different orders. This comparison will illustrate the utility of corrections to the imaginary part of the Green's tensor which were derived in section 4.2.

All simulations have been performed for a transparent dispersionless substrate of permittivity $\epsilon_2 = 2.5$. We have chosen the transition frequency ω_0 to be in the near-UV part of the spectrum. The free-space wavelength corresponding to ω_0 was taken to be $\lambda_0 = 2\pi c/\omega_0 = 300$ nm. The molecular radius was set to $R = 1$ nm and the constant V in (39) was computed as the classical volume occupied by the molecule, i.e., $V = (4\pi/3)R^3$. For simplicity, we have assumed that the molecules have the same height above the substrate. Note however that the matrices W and Σ remain block diagonal even if the molecules have different heights. We have found numerically all six oscillation modes and the respective radiative relaxation rates. However, only the modes polarized along the Y-axis are shown below. There are two such modes and they can be classified as symmetric and anti-symmetric [29]. The symmetric mode has a large overall dipole moment and, correspondingly, a relatively large relaxation rate. We will use the notations Γ_+ and Γ_- for the relaxation rate of the symmetric and the antisymmetric modes, respectively.

We begin with the situation when the molecules are placed directly on the substrate. Specifically, the vertical displacements of the central points $\mathbf{r}_a$ and $\mathbf{r}_b$ are taken to be equal to the molecular radius R: $z_a = z_b = R = 1$ nm. Note that this corresponds to $\mathcal{Z} = 2$ nm. The results are shown in figure 7. It can be seen that, first, the electromagnetic interaction in the system is so strong that the quasi-particle pole approximation is grossly inaccurate. It is important to note that the interaction remains strong even when the intermolecular distance $\mathcal{R}$ is much larger than the molecular radius R. At large distances, the interaction is mediated by the substrate. In the absence of a substrate, the quasi-particle pole approximation is very accurate for $\mathcal{R} \gtrsim 3$ nm (data not shown). Second, even though the vertical displacement from the interface is much smaller than the wavelength at the transition frequency (the characteristic ratio is $1/300$), the electrostatic limiting expression for the Green's tensor is inadequate. This is due to the fact that, as was mentioned above, the radiative corrections appear only at the third order of the expansion (28). Therefore, an accurate description of the radiative processes in the system requires accounting for the terms which are of the third order or higher. For the relaxation rate of the symmetric mode, Γ_+, the third-order approximation to the Green's tensor yields a fairly accurate result (the $n = 3$ curve in figure 7(a)). This can be inferred by

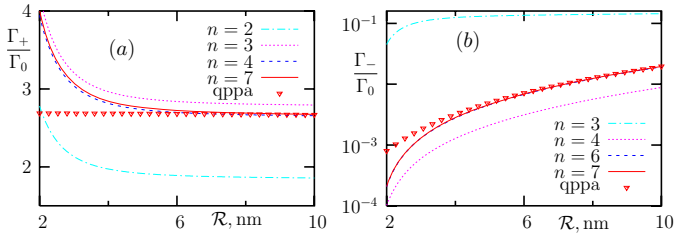

Figure 8. Same as in figure 7 but for $z_a = z_b = 5R = 5$ nm. Additionally, logarithmic vertical scale is used in panel (b).

comparison with the $n = 7$ curve shown on the same plot. Note that the $n = 6$ and $n = 7$ curves are indistinguishable (the $n = 6$ curve is not shown on this graph). For the case of the long-lifetime antisymmetric mode, the third-order approximation to the Green's tensor still yields a grossly inaccurate result (the $n = 3$ curve in figure 7(b)), as expected. An accurate result for Γ_- is obtained by using at least the fifth-order approximation (the $n = 5$ curve). As in the case of the symmetric mode, the $n = 6$ and $n = 7$ curves are indistinguishable which indicates that the obtained results are filly convergent (the $n = 6$ curve is not shown).

Next, consider the case when the molecules are separated from the interface by a distance that is five times larger than in the previously considered figure. Namely, we keep all the parameters unchanged except for the vertical displacements which are now set to be $z_a = z_b = 5R = 5$ nm. The results are shown in figure 8. At this distance from the interface, the electromagnetic interaction which is mediated by the substrate is expected to be weaker. Indeed, it can be seen in figure 8(a) that the quasi-particle pole approximation becomes accurate for the symmetric mode when $\mathcal{R} \gtrsim 5$ nm. For the antisymmetric mode (figure 8(b)), the interaction is even weaker and the quasi-particle pole approximation is accurate for $\mathcal{R} \gtrsim 4$ nm. However, for $\mathcal{R} \sim 2$ nm, the quasi-particle pole approximation yields a relative error of the order of 100%. As was discussed above, the relaxation rate for the symmetric mode must be computed by using at least the third-order approximation to the Green's tensor. However, the $n = 3$ curve in figure 8(a) is still not very accurate. The reason is that, at large distances, the convergence of the short-distance expansion is slower and more terms must be taken into account to obtain an accurate result. The difference is small between the $n = 4$ and $n = 7$ curves and the $n = 6$ and $n = 7$ curves are indistinguishable which indicates that convergence in this case is reached at $n = 4$ (the $n = 6$ curve is not shown). Even slower convergence is obtained for the antisymmetric mode. As can be seen from figure 7(b), the $n = 4$ curve in this case is still very inaccurate and there is a discernible difference between the $n = 5$ and $n = 7$ curves. The $n = 6$ and $n = 7$ curves are still indistinguishable (the $n = 6$ curve is not shown) which indicates that convergence is obtained at $n = 5$ or $n = 6$, depending on the required accuracy.

We note that the $n = 6$ curves were sufficiently accurate in all cases considered above. However, the $n = 7$ results are still needed for verification of convergence if not for improving the accuracy.

7. Summary and discussion

We have derived a short-distance expansion for the half-space Green's tensor. More specifically, we have computed the 'reflected' part of the Green's tensor which is defined above in equations (5), (16) and (17). We have calculated the real part of $\mathcal{G}^R(\mathcal{R}, \mathcal{Z})$ to third

order while the imaginary part, in the special case of a transparent substrate, was obtained to seventh order. The obtained expansion is analogous to the expansion (9) for the free-space Green's tensor and is particularly useful for consideration of radiative processes. While the expansion (9) has proved to be useful in many physical settings and is widely used, an analogous expansion for the reflected Green's tensor has not previously been known.

Analytical results obtained in this paper have been validated numerically for a silver substrate with $\mathcal{R} = 40$ nm and $\mathcal{Z} = 80$ nm in the spectral intervals from $\lambda = 400$ nm to $\lambda = 2\,\mu$m in figure 2 and from 400 nm to 1 cm in figure 3(*b*). We emphasize that the geometry and the spectral interval used in figure 2 are borderline cases. Thus, much better accuracy is obtained for smaller values of $\mathcal{R}$ and $\mathcal{Z}$. An important result that we have obtained is that, even in the case of realistic lossy metal substrates, the imaginary part of the Green's tensor is dominated by radiative corrections which are only obtainable at third order. In particular, the zeroth-order approximation, which coincides with the well-known electrostatic method of images, is grossly inaccurate for the imaginary part of the Green's tensor.

Numerical validation of the short-distance expansion for a glassy substrate is illustrated in figure 4 for the same geometrical parameters and wavelengths as were used in figures 2 and 5. It can be seen that the quality of the approximation is much better in the case of a glassy substrate. We conclude that the accuracy of our expansion is, generally, better for dielectric substrates.

We have also illustrated the utility of the obtained expansion by performing calculations of radiative lifetimes of two identical molecules which are placed in close vicinity of each other above a glassy substrate. It was shown that in the strong interaction regime, the representation of the Green's tensor in terms of the Sommerfeld's integrals is barely usable for the problem under consideration. On the other hand, the analytical expansion derived in this paper can be directly and efficiently used.

Finally, the Fortran-77 codes used in all simulations are available in a supplement to this paper. These codes can be used to compute the Green's tensor from the analytical expansions derived in this paper as well as by computation of the Sommerfeld integrals.

Acknowledgments

This research was supported by the AFOSR under the grant FA9550-07-1-0096 and by the NSF under the grant DMR-0425780.

Appendix A. Derivation of $\mathcal{K}^{(l)}$ to third order

In the appendices, we show detailed derivations only for the zz component of the tensor coefficients $\mathcal{K}^{(l)}$ that appear in this expansion. Computation of other tensor components is carried out by direct analogy. In this appendix, we compute the expansion coefficients up to the order $l = 3$. The calculations are based on the assumption that $\mathcal{R} \sim \mathcal{Z} \sim \mathcal{L}$, where $\mathcal{L}$ is defined by (21). Accordingly, we will write $O(\mathcal{R}) = O(\mathcal{Z}) = O(\mathcal{L})$.

We start from expression (23). Making the change of variables $\sqrt{1-(q/k_1)^2} = \xi$ in the first integral and $\sqrt{(q/k_1)^2 - 1} = \xi$ in the last two integrals, we obtain

$$\mathcal{G}^R_{zz}(\mathcal{R}, \mathcal{Z}) = -k_1^3[\mathrm{i}t_1(\mathcal{R}, \mathcal{Z}) + t_2(\mathcal{R}, \mathcal{Z}) + t_3(\mathcal{R}, \mathcal{Z})], \tag{A.1}$$

where

$$t_1 = \int_0^1 \mathrm{d}\xi (1-\xi^2) \exp(\mathrm{i}\xi k_1 \mathcal{Z}) J_0(k_1 \mathcal{R}\sqrt{1-\xi^2}) Q_1(\xi), \tag{A.2a}$$

$$t_2 = \int_0^\infty \mathrm{d}\xi (1+\xi^2) \exp(-\xi k_1 \mathcal{Z}) J_0(k_1 \mathcal{R}\sqrt{1+\xi^2}) \left[Q_2(\xi) - s - \frac{s(1-s)}{2(1+\xi^2)} \right], \tag{A.2b}$$

$$t_3 = \int_0^\infty \mathrm{d}\xi (1+\xi^2) \exp(-\xi k_1 \mathcal{Z}) J_0(k_1 \mathcal{R}\sqrt{1+\xi^2}) \left[s + \frac{s(1-s)}{2(1+\xi^2)} \right]. \tag{A.2c}$$

Here

$$Q_1(\xi) = \frac{\sqrt{\varepsilon - 1 + \xi^2} - \varepsilon\xi}{\sqrt{\varepsilon - 1 + \xi^2} + \varepsilon\xi}, \qquad Q_2(\xi) = \frac{\sqrt{\xi^2 - \varepsilon + 1} - \varepsilon\xi}{\sqrt{\xi^2 - \varepsilon + 1} + \varepsilon\xi}, \tag{A.3}$$

and ε is defined in (27).

The integral (A.2*a*) is evaluated over the finite interval [0, 1]. A short-distance expansion of this integral can readily be obtained by utilizing the Taylor expansion of the functions $\exp(\mathrm{i}\xi k_1 \mathcal{Z})$ and $J_0(k_1 \mathcal{R}\sqrt{1-\xi^2})$ with respect to the variables $k_1\mathcal{Z}$ and $k_1\mathcal{R}$, respectively. We will compute this integral with the accuracy $O(\mathcal{L}^0)$. This is justified because, as we will see below, the integrals (A.2*b*) and (A.2*c*) contain terms which are of order of $O(\mathcal{L}^{-3})$, $O(\mathcal{L}^{-2})$, $O(\mathcal{L}^{-1})$ and $O(\mathcal{L}^0)$. As can be easily seen,

$$t_1 = \int_0^1 (1-\xi^2) Q_1(\xi)\, \mathrm{d}\xi + O(\mathcal{L}). \tag{A.4}$$

The integral in (A.4) can be evaluated analytically which results in

$$t_1 = -\frac{2\sqrt{\varepsilon-1}}{(\varepsilon-1)(\varepsilon+1)^2} \left\{ \left[\varepsilon(1+3\varepsilon-\varepsilon^2) + \sqrt{\varepsilon-1} \left(\frac{\varepsilon^{5/2}(\sqrt{\varepsilon}+2)}{\sqrt{\varepsilon}+1} - 2\varepsilon - 1 \right) \right] - \frac{3\varepsilon^3}{\sqrt{\varepsilon^2-1}} \ln \left[\frac{(\varepsilon+\sqrt{\varepsilon^2-1})(1+\sqrt{\varepsilon+1})}{\varepsilon+\sqrt{\varepsilon(\varepsilon+1)}} \right] \right\} + O(\mathcal{L}). \tag{A.5}$$

This formula approximates t_1 with the required precision. It can be seen that, at this level of approximation, t_1 is independent of $\mathcal{R}$ and $\mathcal{Z}$ and is therefore of the order of $O(\mathcal{L}^0)$.

With the same accuracy as above, we can write

$$t_2 = \int_0^\infty \mathrm{d}\xi (1+\xi^2) \left[Q_2(\xi) - s - \frac{s(1-s)}{2(1+\xi^2)} \right] + O(\mathcal{L}). \tag{A.6}$$

The integral in (A.6) can be evaluated analytically. We have

$$t_2 = I_1 + I_2 + O(\mathcal{L}), \tag{A.7}$$

where

$$I_1 = \int_0^\infty \mathrm{d}\xi [Q_2(\xi) - s] = \frac{\varepsilon}{(\varepsilon+1)^{3/2}} \left[\pi + \frac{\pi - 2\sqrt{1-\varepsilon^2} - 2\varepsilon \arcsin(\varepsilon)}{\varepsilon - 1} \right] \tag{A.8}$$

and

$$I_2 = \int_0^\infty \mathrm{d}\xi\, \xi^2 \left[Q_2(\xi) - s - \frac{s(1-s)}{2\xi^2} \right] = \frac{\varepsilon}{(1+\varepsilon)^{3/2}} \left\{ \frac{2}{3}\sqrt{1-\varepsilon^2} + \frac{\pi\varepsilon - 2\sqrt{1-\varepsilon^2} - 2\varepsilon \arcsin(\varepsilon)}{(1-\varepsilon^2)} \right\}. \tag{A.9}$$

In the results adduced in section 4, we have used the following logarithmic representation of the function $\arcsin(\varepsilon)$:

$$\arcsin(\varepsilon) = -\mathrm{i} \ln(.\varepsilon + \sqrt{1-\varepsilon^2}). \tag{A.10}$$

The final result for t_2 is

$$t_2 = \frac{\varepsilon}{(1+\varepsilon)^{3/2}}\left[\pi + \frac{2\sqrt{1-\varepsilon^2}}{3} + \frac{\pi + 2i\varepsilon^2 \ln[i\varepsilon + \sqrt{1-\varepsilon^2}] - 2\varepsilon\sqrt{1-\varepsilon^2}}{\varepsilon^2 - 1}\right] + O(\mathcal{L}). \tag{A.11}$$

Next, we need to compute t_3 according to (A.2*c*) with the same accuracy as was used to compute t_1 and t_2. This entails computing the terms in the expansion which are of order $O(\mathcal{L}^{-3})$, $O(\mathcal{L}^{-2})$, $O(\mathcal{L}^{-1})$ and $O(\mathcal{L}^0)$.

We note right away that the approximation we seek cannot be obtained by expanding the Bessel function $J_0(k_1\mathcal{R}\sqrt{1+\xi^2})$ into the Taylor series of its argument. Each term in this expansion is integrable but all the resultant integrals contain terms which are of the order of $O(\mathcal{L}^{-3})$. This is due to the fact that the argument of the Bessel function grows linearly with the integration variable ξ at the upper limit of integration.

We, therefore, adopt here a different approach. We start by writing

$$\sqrt{1+\xi^2} = \xi + \Delta(\xi), \tag{A.12}$$

where

$$\Delta(\xi) = \sqrt{1+\xi^2} - \xi. \tag{A.13}$$

Note that $\Delta(\xi) \leqslant 1$. We then make use of the addition theorem for the Bessel function:

$$J_0(k_1\mathcal{R}\sqrt{1+\xi^2}) = J_0[k_1\mathcal{R}(\xi + \Delta(\xi))] = \sum_{n=-\infty}^{\infty} J_{-n}(k_1\mathcal{R}\xi)J_n[k_1\mathcal{R}\Delta(\xi)]. \tag{A.14}$$

Now the argument $k_1\mathcal{R}\Delta(\xi)$ is bounded and we can expand the Bessel function $J_n[k_1\mathcal{R}\Delta(\xi)]$ in the Taylor series with respect to its argument. From (A.14) we obtain

$$J_0(k_1\mathcal{R}\sqrt{1+\xi^2}) = J_0(k_1\mathcal{R}\xi) - k_1\mathcal{R}\Delta(\xi)J_1(k_1\mathcal{R}\xi) + O(\mathcal{L}^2). \tag{A.15}$$

This holds uniformly for all values of ξ. Note that if we keep only the first term in this expression, that is, write approximately $J_0(k_1\mathcal{R}\sqrt{1+\xi^2}) \approx J_0(k_1\mathcal{R}\xi)$ and disregard the contributions to the Green's tensor given by t_1 and t_2, we would arrive at the well-known electrostatic limit (the dipole reflection formula). Account of the terms t_1 and t_2, and of the second term in (A.15) yields us the corrections to the electrostatic limit that we are seeking.

Upon substitution of (A.15) into (A.2*c*), we obtain

$$t_3 = \frac{s}{(k_1\mathcal{L})^3}\left[3\left(\frac{\mathcal{Z}}{\mathcal{L}}\right)^2 - 1\right] - \left[s + \frac{s(1-s)}{2}\right]\left[\frac{1}{k_1\mathcal{L}} + I_3\right] - sI_4 + O(\mathcal{L}), \tag{A.16}$$

where

$$I_3 = k_1\mathcal{R}\int_0^\infty \mathrm{d}\xi\, \Delta(\xi)\exp(-\xi k_1\mathcal{Z})J_1(k_1\mathcal{R}\xi), \tag{A.17}$$

$$I_4 = k_1\mathcal{R}\int_0^\infty \mathrm{d}\xi\, \xi^2\Delta(\xi)\exp(-\xi k_1\mathcal{Z})J_1(k_1\mathcal{R}\xi). \tag{A.18}$$

Note that in the derivation of (A.16) we have used the following formulae:

$$\int_0^\infty \mathrm{d}\xi \exp(-a\xi)J_0(b\xi) = \frac{1}{\sqrt{a^2+b^2}}, \tag{A.19}$$

$$\int_0^\infty \mathrm{d}\xi\, \xi^2 \exp(-a\xi)J_0(b\xi) = \frac{1}{(a^2+b^2)^{3/2}}\left(\frac{3a^2}{a^2+b^2} - 1\right) \qquad (\text{for } a, b > 0). \tag{A.20}$$

The remaining integrals, I_3 and I_4, can be estimated as follows. First, we show that $I_3 = O(\mathcal{L})$ and, therefore, can be neglected. Indeed, I_3 is convergent when $\mathcal{Z} = 0$, so that we can write

$$I_3 = [1 + O(\mathcal{L})]k_1\mathcal{R}\int_0^\infty \mathrm{d}\xi\,\Delta(\xi)J_1(k_1\mathcal{R}\xi). \tag{A.21}$$

Using the relation $J_1(\xi) = -\mathrm{d}J_0(\xi)/\mathrm{d}\xi$ and integrating by parts, we obtain

$$I_3 = [1 + O(\mathcal{L})]\left[1 + \int_0^\infty J_0(k_1\mathcal{R}\xi)\,\mathrm{d}\Delta(\xi)\right]. \tag{A.22}$$

This integral converges when $\mathcal{R} = 0$. Therefore we can expand the Bessel function $J_0(k_1\mathcal{R}\xi)$ and write with the required precision

$$I_3 = [1 + O(\mathcal{L})]\big[1 + \Delta(\xi)\big|_0^\infty + O\mathcal{L}\big] = [1 + O(\mathcal{L})]O(\mathcal{L}) = O(\mathcal{L}). \tag{A.23}$$

Finally, the integral in (A.18) can be rewritten with the use of the identity $\Delta(\xi) = \sqrt{1+\xi^2} - \xi = 1/(\sqrt{1+\xi^2}+\xi)$ as

$$\begin{aligned} I_4 &= k_1\mathcal{R}\int_0^\infty \mathrm{d}\xi\,\xi^2\left(\frac{1}{\sqrt{1+\xi^2}+\xi} - \frac{1}{2\xi} + \frac{1}{2\xi}\right)J_1(k_1\mathcal{R}\xi)\exp(-k_1\mathcal{Z}\xi) \\ &= I_4^{(a)} + I_4^{(b)}, \end{aligned} \tag{A.24}$$

where

$$I_4^{(a)} = k_1\mathcal{R}\int_0^\infty \mathrm{d}\xi\,\xi^2\left[\frac{1}{\sqrt{1+\xi^2}+\xi} - \frac{1}{2\xi}\right]J_1(k_1\mathcal{R}\xi)\exp(-\xi k_1\mathcal{Z}), \tag{A.25a}$$

$$I_4^{(b)} = \frac{1}{2}k_1\mathcal{R}\int_0^\infty \mathrm{d}\xi\,\xi J_1(k_1\mathcal{R}\xi)\exp(-\xi k_1\mathcal{Z}). \tag{A.25b}$$

It can be shown that, analogously to the case of I_3, the integral $I_4^{(a)}$ is of the order of $O(\mathcal{L})$ and can be neglected. The proof is analogous to the case of I_3 and is omitted. The last integral, $I_4^{(b)}$, can be computed exactly; the result reads $I_4^{(b)} = \mathcal{R}^2/2k_1\mathcal{L}^3$. Therefore, we have computed the integral I_4 with the required precision:

$$I_4 \approx \frac{\mathcal{R}^2}{2k_1\mathcal{L}^3}. \tag{A.26}$$

The final result for t_3 is

$$t_3 = \frac{s}{(k_1\mathcal{L})^3}\left[3\left(\frac{\mathcal{Z}}{\mathcal{L}}\right)^2 - 1\right] - \frac{1}{k_1\mathcal{L}}\left[s + \frac{s(1-s)}{2}\right] - \frac{s\mathcal{R}^2}{2k_1\mathcal{L}^3} + O(\mathcal{L}). \tag{A.27}$$

We now substitute (A.5), (A.11) and (A.27) into (A.1) and arrange all the terms in the resultant expression according to the order of magnitude. This leads to the formulae listed in section 4 for the expansion coefficients $\mathcal{K}_{zz}^{(l)}$ for $l = 0, 1, 2, 3$.

Appendix B. Calculation of $\mathrm{Im}\,\mathcal{K}^{(l)}$ to seventh order for transparent substrates

We now consider the special case when the substrate is a transparent dielectric whose permittivity ϵ_2 is purely real. Correspondingly, we assume that $\varepsilon = \epsilon_2/\epsilon_1$ is also real. Then it is possible to compute higher-order corrections to $\mathrm{Im}\,\mathcal{G}^R$. In this appendix, we illustrate this for the specific tensor component $\mathcal{G}_{zz}^R$.

It follows from (A.1) that

$$\mathrm{Im}\big(\mathcal{G}^R_{zz}\big) = -k_1^3[\mathrm{Re}(t_1) + \mathrm{Im}(t_2)], \tag{B.1}$$

where t_1 and t_2 are defined in equations (A.2*a*) and (A.2*b*) of appendix A. Assume for the moment that $\varepsilon \geqslant 1$. In this case, t_1 is real while

$$\mathrm{Im}(t_2) = \int_0^{\sqrt{\varepsilon-1}} \mathrm{d}\xi (1+\xi^2) \exp(-\xi k_1 \mathcal{Z}) J_0(k_1 \mathcal{R}\sqrt{1+\xi^2}) \mathrm{Im}\, Q_2(\xi). \tag{B.2}$$

We now use (A.3) to evaluate $\mathrm{Im}\, Q_2(\xi)$. This yields

$$\mathrm{Im}\, Q_2(\xi) = -\frac{2\varepsilon\xi\sqrt{\varepsilon-1+\xi^2}}{\xi^2(\varepsilon^2-1)+\varepsilon-1}. \tag{B.3}$$

We then expand the exponential and the Bessel function in (B.2) and (A.2*a*) in a power series and use equations (B.3) and (A.3) to obtain

$$\mathrm{Im}\, \mathcal{K}^{(4)}_{zz} = -2\varepsilon(\varepsilon-1)\frac{\mathcal{Z}}{\mathcal{L}} \int_0^1 \mathrm{d}\xi\, \xi^2 f_3(\xi), \tag{B.4a}$$

$$\mathrm{Im}\, \mathcal{K}^{(5)}_{zz} = \frac{\mathcal{Z}^2}{\mathcal{L}^2}\left\{\frac{1}{2}\int_0^1 \mathrm{d}\xi\, \xi^2(1-\xi^2)Q_1(\xi) + \varepsilon(\varepsilon-1)^{3/2}\int_0^1 \mathrm{d}\xi\, \xi^3 f_3(\xi)\right\}$$
$$-\frac{\mathcal{R}^2}{\mathcal{L}^2}\left\{\frac{1}{4}\int_0^1 \mathrm{d}\xi (1-\xi^2)^2 Q_2(\xi) - \frac{\varepsilon(\varepsilon-1)^{1/2}}{2}\int_0^1 \mathrm{d}\xi\, \xi f_2(\xi) f_3(\xi)\right\}, \tag{B.4b}$$

$$\mathrm{Im}\, \mathcal{K}^{(6)}_{zz} = -\frac{\mathcal{Z}^3\varepsilon(\varepsilon-1)^2}{3\mathcal{L}^3}\int_0^1 \mathrm{d}\xi\, \xi^4\sqrt{1-\xi^2}[1+f_1(\xi)] + \frac{\mathcal{Z}\mathcal{R}^2\varepsilon(\varepsilon-1)}{2\mathcal{L}^3}\int_0^1 \mathrm{d}\xi\, \xi^4 f_3(\xi), \tag{B.4c}$$

$$\mathrm{Im}\, \mathcal{K}^{(7)}_{zz} = \frac{\mathcal{Z}^4}{\mathcal{L}^4}\left\{-\frac{1}{24}\int_0^1 \mathrm{d}\xi\, \xi^4(1-\xi^2)Q_1(\xi) + \frac{\varepsilon(\varepsilon-1)^{5/2}}{12}\int_0^1 \mathrm{d}\xi\, \xi^5 f_3(\xi)\right\}$$
$$-\frac{\mathcal{Z}^2\mathcal{R}^2}{\mathcal{L}^4}\left\{\frac{1}{8}\int_0^1 \mathrm{d}\xi\, \xi^2(1-\xi^2)^2 Q_1(\xi) + \frac{\varepsilon(\varepsilon-1)^{3/2}}{4}\int_0^1 \mathrm{d}\xi\, \xi^3 f_2(\xi) f_3(\xi)\right\}$$
$$+\frac{\mathcal{R}^4}{\mathcal{L}^4}\left\{-\frac{1}{64}\int_0^1 \mathrm{d}\xi (1-\xi^2)^3 Q_1(\xi) + \frac{\varepsilon(\varepsilon-1)^{1/2}}{32}\int_0^1 \mathrm{d}\xi\, \xi f_2^2(\xi) f_3(\xi)\right\}. \tag{B.4d}$$

Here

$$f_1(\xi) = \frac{\varepsilon(\varepsilon-1)\xi^2}{\xi^2(\varepsilon^2-1)+1}, \qquad f_2(\xi) = 1+(\varepsilon-1)\xi^2, \qquad f_3(\xi) = \frac{f_2(\xi)\sqrt{1-\xi^2}}{\xi^2(\varepsilon^2-1)+1}. \tag{B.5}$$

The above integrals can be computed analytically. The results are given in section 4.2. Note that, by utilizing similar expansions, it is possible to show that the obtained formulae are also valid when $0 < \varepsilon \leqslant 1$. Therefore, the corrections of section 4.2 are valid if $\varepsilon > 0$.

Appendix C. The functions $r_k(x)$ and $p_k(x)$

The formulae given in section 4.2 contain rational functions $r_k(x)$ $(k = 1, \ldots, 13)$ and polynomials $p_k(x)$ $(k = 1, \ldots, 7)$, which are defined in this appendix.

All functions $r_k(x)$ have a common denominator and can be written as

$$r_k(x) = \frac{\pi_k(x)}{x+1}, \tag{C.1}$$

where $\pi_k(x)$ are the following polynomials:

$$\pi_1(x) = 4x^{10} + 4x^9 + 4x^8 + 8x^7 - 14x^6 + 2x^5 - 21x^4 + 11x^3 - 9x^2 - 2x - 2,$$
$$\pi_2(x) = x^2(8x^8 + 8x^7 + 26x^6 + 18x^5 + 15x^4 - 33x^3 - x^2 + 2x + 2),$$
$$\pi_3(x) = 8x^{10} + 8x^9 + 30x^8 + 14x^7 + 29x^6 - 19x^5 - 3x^4 - 18x^3 - 18x^2 - 8x - 8,$$
$$\pi_4(x) = 2x^{10} + 2x^9 + 6x^8 + 5x^7 + 2x^6 - 10x^5 + 3x^3 + 3x^2 + x + 1,$$
$$\pi_5(x) = 2x^{10} + 2x^9 + 11x^8 + 15x^7 + 7x^6 - 10x^5 - 10x^4 - 12x^3 - 12x^2 - 4x - 4,$$
$$\pi_6(x) = 16x^{14} + 16x^{13} + 16x^{12} + 16x^{11} - 52x^{10} - 70x^9 - 30x^8 - 120x^7 + 154x^6 - 34x^5 + 183x^4 - 77x^3 + 63x^2 + 12x + 12,$$
$$\pi_7(x) = 32x^{14} + 32x^{13} + 80x^{12} + 80x^{11} - 24x^{10} - 8x^9 - 246x^8 - 150x^7 - 177x^6 + 191x^5 - 33x^4 - 38x^3 - 38x^2 - 8x - 8,$$
$$\pi_8(x) = x^2(48x^{12} + 48x^{11} + 200x^{10} + 200x^9 + 298x^8 + 250x^7 + 7x^6 - 425x^5 - 137x^4 + 10x^3 + 10x^2 + 8x + 8),$$
$$\pi_9(x) = x^2(32x^{12} + 32x^{11} + 96x^{10} + 96x^9 + 40x^8 + 64x^7 - 154x^6 - 50x^5 - 187x^4 + 37x^3 - 75x^2 - 18x - 18),$$
$$\pi_{10}(x) = 48x^{14} + 48x^{13} + 232x^{12} + 232x^{11} + 482x^{10} + 338x^9 + 443x^8 - 85x^7 + 11x^6 - 382x^5 - 382x^4 - 344x^3 - 344x^2 - 96x - 96,$$
$$\pi_{11}(x) = 8x^{14} + 8x^{13} + 18x^{12} + 18x^{11} - 14x^{10} - 11x^9 - 73x^8 - 50x^7 - 43x^6 + 67x^5 - 3x^4 - 12x^3 - 12x^2 - 3x - 3,$$
$$\pi_{12}(x) = 8x^{14} + 8x^{13} + 32x^{12} + 32x^{11} + 42x^{10} + 38x^9 - 17x^8 - 85x^7 - 29x^6 + 18x^5 + 18x^4 + 16x^3 + 16x^2 + 4x + 4,$$
$$\pi_{13}(x) = 8x^{14} + 8x^{13} + 46x^{12} + 46x^{11} + 133x^{10} + 157x^9 + 109x^8 - 50x^7 - 50x^6 - 136x^5 - 136x^4 - 96x^3 - 96x^2 - 24x - 24.$$

The polynomials $p_k(x)$ are defined as

$$p_1(x) = 2x^3 + 5x^2 + 1,$$
$$p_2(x) = x^2 + 6x + 1,$$
$$p_3(x) = 2x^5 + 5x^4 - 8x^2 + 2x - 1$$
$$p_4(x) = 4x^5 + 17x^4 + 22x^3 - 14x^2 + 2x + 1,$$
$$p_5(x) = 4x^5 + 19x^4 + 34x^3 + 22x^2 + 14x + 3,$$
$$p_6(x) = x^4 + 4x^3 + 4x^2 - 8x - 1$$
$$p_7(x) = x^4 + 6x^3 + 18x^2 + 6x + 1.$$

References

[1] Sommerfeld A 1909 *Ann. Phys. Lpz.* **28** 665
[2] Maradudin A A and Mills D L 1975 *Phys. Rev.* B **11** 1392–415
[3] Tai C 1994 *Dyadic Green Functions in Electromagnetic Theory* (New York: IEEE Press)
[4] Novotny L and Hecht B 2006 *Principles of Nano-Optics* (Cambridge: Cambridge University Press)
[5] Hecht B, Bielefeldt H, Inouye Y, Pohl D W and Novotny L 1997 *J. Appl. Phys.* **81** 2492–8
[6] Greffet J J and Carminati R 1997 *Prog. Surf. Sci.* **56** 133–237
[7] Bozhevolnyi S I 1997 *J. Opt. Soc. Am.* B **14** 2254–9
[8] Bozhevolnyi S I 2000 Near-field optics of nanostructured surfaces *Optics of Nanostructured Materials* (*Wiley Series in Lasers and Applications*) (New York: Wiley-Interscience) pp 355–412
[9] Carney P S and Schotland J C 2000 *Appl. Phys. Lett.* **77** 2798–80

[10] Carney P S, Markel V A and Schotland J C 2001 *Phys. Rev. Lett.* **86** 5874–7
[11] Carney P S and Schotland J C 2001 *Opt. Lett.* **26** 1072–4
[12] Carney P S and Schotland J C 2002 *J. Opt.* A **4** S140–4
[13] Carney P S and Schotland J C 2003 *J. Opt. Soc. Am.* A **20** 542–7
[14] Carney P S, Frazin R A, Bozhevolnyi S I, Volkov V S, Boltasseva A and Schotland J C 2004 *Phys. Rev. Lett.* **92** 163903
[15] Sun J, Carney P S and Schotland J C 2006 *IEEE J. Sel. Top. Quantum Electron.* **12** 1072–83
[16] Brongersma M L, Hartman J W and Atwater H A 2000 *Phys. Rev.* B **62** R16356–R16359
[17] Maier S A, Kik P G and Atwater H A 2002 *Appl. Phys. Lett.* **81** 1714–6
[18] Maier S A, Kik P G, Atwater H A, Meltzer S, Harel E, Koel B E and Requicha A G 2003 *Nature Mater.* **2** 229–32
[19] Crozier K B, Togan E, Simsek E and Yang T 2007 *Opt. Express* **15** 17482–93
[20] Markel V A and Sarychev A K 2007 *Phys. Rev.* B **75** 085426
[21] Govyadinov A A and Markel V A 2008 *Phys. Rev.* B **78** 035403
[22] Gartstein Y N and Agranovich V M 2007 *Phys. Rev.* B **76** 115329
[23] Chance R R, Prock A and Silbey R 1978 *Adv. Chem. Phys.* **37** 1
[24] Anger P, Bharadwaj P and Novotny L 2006 *Phys. Rev. Lett.* **96** 113002
[25] Carminati R, Greffet J J, Henkel C and Vigoureux J M 2006 *Opt. Comm.* **61** 368–75
[26] Joulain K, Mulet J P, Marquier F, Carminati R and Greffet J J 2005 *Surf. Sci. Rep.* **57** 59–112
[27] Taubenblatt M A and Tran T K 1993 *J. Opt. Soc. Am.* A **10** 912–9
[28] Markel V A 1992 *J. Mod. Opt.* **39** 853–61
[29] Markel V A 1995 *J. Opt. Soc. Am.* B **12** 1783–91
[30] Danilova Y E, Markel V A and Safonov V P 1993 *Atmos. Oceanic Opt.* **6** 821–6
[31] Draine B T and Goodman J 1993 *Astrophys. J.* **405** 685–97
[32] Scully M O and Zubairy M S 1997 *Quantum Optics* (Cambridge: Cambridge University Press)
[33] Markel V A 2006 *J. Phys.: Condens. Matter* **18** 11149–65
[34] Rowland T Companion matrix *MathWorld—A Wolfram Web Resource* ed E W Weisstein http://mathworld.wolfram.com/CompanionMatrix.html